Analyses of the Scattering of Nuclear Particles by Collective Nuclei in Terms of the Coupled-Channel Calculation*

TARO TAMURA

Oak Ridge National Laboratory, Oak Ridge, Tennessee

The formalism of the coupled-channel analysis of the scattering of nuclear projectiles by nuclei is presented in detail. Since the necessity for coupled-channel calculations increases with the degree of collectivity exhibited by the target nucleus, the presentation is particularly suited to collective nuclei, with the target states described by phenomenological collective coordinates. Within this restriction the formalism given here is quite general so that the following cases can be considered: The target can be any (collective) nucleus, even-A or odd-A, vibrational or rotational; the projectile can be either charged or uncharged, and can have any spin; either or both the projectile and the target can be polarized; finally, the energy of the projectile can be very low since the contribution of the compound-state formation to the cross section can be included. Using a computer program which was written following the above formalism (which can be used to do any of the calculations enumerated above) scattering cross sections for several typical cases were obtained and are presented to show their contrasting behavior when different targets (and different coupling schemes) and different projectiles are chosen. Realistic calculations were also made in order to fit a large number of existing experimental data. Good fits were obtained in most cases which indicates that the coupled-channel calculation is a very powerful tool in explaining various complicated scattering data, and further in extracting useful spectroscopic informations about the target nucleus. Possible future developments of the present analyses are discussed.

I. INTRODUCTION

In recent years a large amount of experimental data has been accumulated on various types of nuclear reactions such as elastic and inelastic scattering and transmutation reactions caused by medium- and low-energy nuclear particles (nucleons, deuterons, α particles, and so forth). Many of these data have been successfully described by the distorted-wave Born approximation (DWBA).[1a] The reason for the success of DWBA lies in the fact that the interaction which causes these reactions is usually comparatively weak, so the first-order perturbation treatment is a good approximation.

In treating inelastic scattering, special care must be exercised, compared to the treatment of transmutation reactions. In some cases the inelastic-scattering cross sections have rather large magnitudes, indicating that the interactions involved there are sometimes much stronger than those in transmutation reactions, and thus that DWBA might become a poor approximation. Such a situation is often met when the target nucleus is of a collective nature.

When the DWBA turns out to be poor, one conceivable improvement is to include the second and higher Born approximations. However, to perform such higher-order calculations is a rather involved task.

Another possible improvement to DWBA is the coupled-channel calculation.[2] In such calculations the

* Research sponsored by the U.S. Atomic Energy Commission under contract with the Union Carbide Corporation.

[1] (a) See, e.g., R. H. Bassel, G. R. Satchler, R. M. Drisco, and E. Rost, Phys. Rev. **110**, 1080 (1958) and many other papers which followed. Concerning the comparison of the DWBA to the coupled-channel calculations, see F. G. Perey and G. R. Satchler, Phys. Letters **5**, 212 (1963). (b) E. V. Inopin, Zh. Eksperim. i Teor. Fiz. **31**, 901 (1956) [English transl.: Soviet Phys.—JETP **4**, 784 (1957)]; J. S. Blair, Phys. Rev. **115**, 928 (1958); J. S. Blair, D. Sharp, and L. Wilets, *ibid.* **125**, 1625 (1962). See also N. Austern and J. S. Blair (to be published), who discuss the higher-order Born approximation, particularly in combination with the strong-absorption model. (c) For the validity of the strong-absorption model in comparison with experiment, see J. S. Blair, "Nuclear Spectroscopy with Direct Reactions II," Argonne National Laboratory Report 1964 ANL-6878 (unpublished), p. 143.

[2] A. Bohr and B. R. Mottelson, Kgl. Danske Videnskab. Selskab, Mat. Fys. Medd. **27**, No. 16 (1953).

interactions are considered to infinite order in the sense that, although one restricts the number of channels to be considered to a finite number, the interaction is treated exactly within the channels considered. As is expected, and as shown in the following, the restriction of the number of channels is not a bad approximation if we are interested in the explanation of the excitation of a limited number of lower excited states.

There is another big advantage in the use of the coupled-channel calculations over the DWBA. In many nuclei there are low-lying states that have strong collective natures, but the inelastic cross sections to them are not necessarily very large. These are, for example, the higher phonon states in vibrational nuclei, or the higher members of the rotational bands of deformed nuclei. The excitation of these states is caused via the excitation of the states that lie at lower energies. In other words, their excitation cannot be caused through single-step processes. If such multiple processes are to be treated in terms of perturbation theory, it has to be made through the higher-order Born approximations. However the formulation and (when one attempts to use a computer for the numerical analysis) the programming become progressively more involved each time one increases the order of the approximation. In the coupled-channel calculations, such processes can be treated by simply increasing the number of the coupled channels. Furthermore, in this calculation the formulation, and consequently the coding of the computer program, is essentially the same irrespective of how many channels one takes into account and thus can be handled comparatively easily.

When the target nucleus is of a collective nature, and when the projectile is strongly absorptive, another approximation, the strong-absorption model which was proposed by Inopin and extended by Blair[1b] can be used. In this the cross section is expressed in a very compact form and thus very little numerical calculation is needed for its evaluation. It also gives good agreement with experiments,[1c] at least for the excitation of states which are excited with single-step processes from the ground state. However, this theory does not seem to be as flexible as the coupled-channel calculation. For example, when the collective states are described, not phenomenologically by introducing the collective coordinates, but in terms of the particle aspects, it is difficult for this theory to apply, while the coupled-channel calculation can still be used. Also, this theory cannot be used to describe the scattering of weakly absorptive particles, like nucleons. On the other hand the coupled-channel calculation can be applied for both strongly and weakly absorptive projectiles.

The importance of the coupled-channel calculation in describing scattering processes when the target nuclei are of collective nature was first pointed out by Bohr and Mottelson,[2] and then was applied by Margolis *et al.* and Chase *et al.*[3] in computing the strength functions of very slow neutrons. The application of this idea to the description of the inelastic, as well as elastic, scattering of higher-energy incident particles was first made by Yoshida,[4] although he performed numerical calculations only under very restricted assumptions.

Because of the success of the optical-model analysis[5] of the elastic scattering of various particles by various nuclei, and the easier access to high-speed computers, more realistic numerical analyses of the scattering processes based on the coupled-channel calculation have become meaningful and feasible. Thus, Buck[6,7] showed that with this method it is, in fact, possible to fit the experimental differential cross sections of both the elastic and inelastic scattering of protons and α particles by various collective nuclei.

However, Buck's calculations were limited to the cases in which the target nucleus is of even A and only two or three states in the target are coupled together. On the other hand, there have accumulated a number of experimental data which use odd-A as well as even-A nuclei as targets, and give differential cross sections of the inelastic scattering to various higher excited states. It was therefore important to extend Buck's work so that such experimental data could also be analyzed theoretically.

The present paper reports on such an extension, both in formulation and in the analyses of various new experimental data. As has already been reported on various occasions[8–13] and is summarized in Sec. VII, the coupled-channel analysis is indeed quite powerful; many experimental data were well fitted by our calculations and spectroscopic information about the target states was derived from such fitting.

Our formulation of the calculation (and the corresponding coding of the computer program) have been made in a very general way, so that a variety of scattering calculations can be made easily. Thus in Sec. II we start with quite general optical-model potentials, which are usually nonspherical. These potentials are then re-expressed in some approximate ways, the way depending on the nature of the target, and

[3] B. Margolis and E. S. Troubetzksy, Phys. Rev. **106,** 105 (1957). D. M. Chase, L. Wilets, and A. R. Edmonds, Phys. Rev. **110,** 1080 (1958).
[4] S. Yoshida, Proc. Phys. Soc. (London) **A69,** 668 (1956).
[5] R. D. Woods and D. S. Saxon, Phys. Rev. **95,** 577 (1954).
[6] B. Buck, Phys. Rev. **127,** 940 (1962).
[7] B. Buck, Phys. Rev. **130,** 712 (1963). See also B. Buck, A. P. Stamp, and P. E. Hodgson, Phil. Mag. **8,** 1805 (1963).
[8] J. K. Dickens, F. G. Perey, R. J. Silva, and T. Tamura, Phys. Letters **6,** 53 (1963).
[9] T. Tamura, Phys. Letters **9,** 334 (1964).
[10] M. Sakai and T. Tamura, Phys. Letters **10,** 323 (1964).
[11] G. C. Pramila, R. Middleton, T. Tamura, and G. R. Satchler, Nucl. Phys. **61,** 448 (1965).
[12] R. Wagner, P. D. Miller, T. Tamura, and H. Marshak, Phys. Letters **10,** 316 (1964).
[13] T. Tamura, Phys. Letters **12,** 121 (1964).

thus terms which cause the coupling between different channels are derived explicitly. Because of these coupling terms, the Schrödinger equation, which describes the scattering, becomes a set of coupled differential equations, which is derived in Sec. III. If these coupled equations are solved and the solutions are matched to appropriately defined asymptotic solutions, one gets a set of S-matrix elements. These elements are then used in computing various cross sections, as explained in Sec. IV. The contents of Sec. II through IV thus complete the formulation of our calculation for general cases. When, however, the target nucleus is well deformed and the energy of the incident particle is sufficiently high, one can perform the calculation more easily by using the adiabatic approximation.[14,15] We therefore give in Sec. V a formalism appropriate to this approximation. Section VI is devoted to a brief account of how various (theoretical) cross sections behave when various types of coupling are considered or various values are taken for the parameters involved. The results of the more realistic numerical calculations and their comparison with experiments are summarized in Sec. VII. Finally in Sec. VIII we discuss suggestions for future work, both theoretical and experimental.

II. THE INTERACTION POTENTIAL

The contents of this and the following three sections are not all new. Rather similar formulations have already been given by various authors.[2–4,6,7,15] Nevertheless, in each of these works only a very limited case has been considered, and thus it is worthwhile to give here the general expressions and formulas in some detail so that the piecewise information given in these works are summarized and their extension can be understood clearly.

As is easily seen, the coupled-channel calculation is required to be made only when the (direct or indirect) couplings between the excited- and the ground-state channels are strong, that is to say only when the low-lying states of the target nucleus have a strong collective nature. Such collective motions can be described fairly well in terms of the (permanent or vibrational) deformations of the nuclear shape. In this view, the description of the coupling potentials between channels can be made in a simple and rather unambiguous way.

Throughout the present work, we use this phenomenological description, and thus assume that the whole interaction to which an incident particle is subject is described by an optical-model potential $V(r, \theta, \phi)$ which is, in general, nonspherical. This potential is usually complex and includes the spin–orbit interaction and also the Coulomb interaction if the incident particle is charged. As for the radial dependence of the potential, we assume that of the Saxon–Woods[4] form and its derivative. Thus explicitly we assume that

$$V(r,\theta,\phi)=-(V+iW)\frac{1}{1+\exp[(r-R)/a]}$$
$$-4iW_D\frac{\exp[(r-\bar{R})/\bar{a}]}{\{1+\exp[(r-\bar{R})/\bar{a}]\}^2}-V_{so}(\boldsymbol{\sigma}\cdot\mathbf{l})\lambda_\pi{}^2\frac{1}{ar}$$
$$\cdot\frac{\exp[(r-R)/a]}{\{1+\exp[(r-R)/a]\}^2}+V_{\text{Coul}},$$

($\lambda_\pi=\pi$-meson Compton wavelength). (1)

The Coulomb interaction V_{Coul} is given explicitly later.

Equation (1) is the same as in Buck.[7] The potential used by Chase *et al.*[3] is similar, but simpler than Eq. (1). If R and $\bar{R}$ are taken independent of the angle, Eq. (1) is nothing but the usual optical-model potential, as used for example by Perey,[16] but we make R and $\bar{R}$ dependent on the polar angles θ and ϕ, in accord with the phenomenological description mentioned above. Their dependence is to be determined according to the collective nature of the target nucleus considered[2]; if the target nucleus is spherically symmetric, but is susceptible to vibration around that spherical shape, R and $\bar{R}$ may be expressed as

$$R=R_0\Big(1+\sum_{\lambda\mu}\alpha_{\lambda\mu}Y_{\lambda\mu}(\theta,\phi)\Big),$$
$$\bar{R}=\bar{R}_0\Big(1+\sum_{\lambda\mu}\alpha_{\lambda\mu}Y_{\lambda\mu}(\theta,\phi)\Big). \quad (2)$$

On the other hand, if the target is an (axially symmetric) deformed nucleus, they are written as

$$R=R_0\Big(1+\sum_{\lambda}\beta_\lambda Y_{\lambda0}(\theta')\Big),$$
$$\bar{R}=\bar{R}_0\Big(1+\sum_{\lambda}\beta_\lambda Y_{\lambda0}(\theta')\Big). \quad (3)$$

In (2) and (3), $R_0=r_0A^{\frac{1}{3}}$ and $\bar{R}_0=\bar{r}_0A^{\frac{1}{3}}$, where A is the mass number of the target. In (3) the angle θ' refers to the body-fixed system.

Since it is impractical to solve the scattering problem subject to the potential (1) with (2) or (3), we now make the following (plausible) approximations.

(i) For the vibrational nucleus we insert (2) into (1) and expand the latter in powers of $\sum_{\lambda\mu}\alpha_{\lambda\mu}Y_{\lambda\mu}$. By defining e and $\bar{e}$ by

$$e=\exp[(r-R_0)/a],$$
$$\bar{e}=\exp[(r-\bar{R}_0)/\bar{a}], \quad (4)$$

and taking the series up to the second order of

[14] S. I. Drozdov, Zh. Eksperim. i Teor. Fiz. **28**, 734, 736 (1955) [English transl.: Soviet Phys.—JETP **1**, 588, 591 (1955)].
[15] B. C. Barrett, Nucl. Phys. **51**, 27 (1964).
[16] F. G. Perey, Phys. Rev. **131**, 745 (1963); Paper C2, "Symposium on Nuclear Spectroscopy with Direct Reactions," Argonne National Laboratory Report ANL-6848, 1964 (unpublished).

$\sum_{\lambda\mu}\alpha_{\lambda\mu}Y_{\lambda\mu}$, we get

$$V(r,\theta,\phi)=-(V+iW)(1+e)^{-1}-4iW_D\bar{e}(1+\bar{e})^{-2}$$
$$-V_{SO}(\boldsymbol{\sigma}\cdot\mathbf{l})(\lambda_\pi^2/ar)e(1+e)^{-2}$$
$$-\{(V+iW)(R_0/a)e(1+e)^{-2}$$
$$-4iW_D(\bar{R}_0/\bar{a})\bar{e}(1-\bar{e})(1+\bar{e})^{-3}\}\sum_{\lambda\mu}\alpha_{\lambda\mu}Y_{\lambda\mu}$$
$$+\{(V+iW)(R_0^2/2a^2)e(1-e)(1+e)^{-3}$$
$$-4iW_D(\bar{R}_0^2/2\bar{a}^2)\bar{e}(1-4\bar{e}+\bar{e}^2)(1+\bar{e})^{-4}\}$$
$$\cdot(\sum_{\lambda\mu}\alpha_{\lambda\mu}Y_{\lambda\mu})^2+V_{\text{Coul}}. \quad (5)$$

We can use the following relation in (5):

$$(\sum_{\lambda\mu}\alpha_{\lambda\mu}Y_{\lambda\mu})^2=\sum_{\lambda\lambda'\lambda''}[\hat{\lambda}'\hat{\lambda}''/(4\pi)^{\frac{1}{2}}\hat{\lambda}](\lambda'\lambda''00\mid\lambda0)$$
$$\times\sum_{\mu}Y_{\lambda\mu}(\alpha_{\lambda'}\otimes\alpha_{\lambda''})_{\lambda\mu}, \quad (6)$$

where $\hat{\lambda}=(2\lambda+1)^{\frac{1}{2}}$, while the symbol $\otimes$ means the vector addition, i.e.,

$$(\alpha_{\lambda'}\otimes\alpha_{\lambda''})_{\lambda\mu}=\sum_{\mu\mu'}(\lambda'\lambda''\mu'\mu''\mid\lambda\mu)\alpha_{\lambda'\mu'}\alpha_{\lambda''\mu''}.$$

We now specify the Coulomb interaction, following Satchler *et al.*[17] as

$$V_{\text{Coul}}=ZZ'\epsilon^2\int\rho(r',\theta',\phi')(|\mathbf{r}-\mathbf{r}'|)^{-1}\,d\mathbf{r}'$$
$$=4\pi ZZ'\epsilon^2\sum_{\lambda\mu}\int\rho(r',\theta',\phi')(2\lambda+1)^{-1}r_<^{\lambda}r_>^{-(\lambda+1)}$$
$$\cdot Y_{\lambda\mu}(\theta,\phi)Y_{\lambda\mu}^*(\theta',\phi')r'^2\,dr'\,d\Omega'. \quad (7)$$

Here $Z\epsilon$ and $Z'\epsilon$ are the charges of the projectile and the target, respectively, while $\rho(r',\theta',\phi')$ gives the charge distribution in the target, which with a reasonable accuracy may be assumed to be constant within the Coulomb radius $R_c(\theta',\phi')$ and zero outside. Thus ρ is written as

$$\rho(r',\theta',\phi')=(3/4\pi R_c^3)\theta(R_c(\theta',\phi')-r'), \quad (8)$$

where $\theta(r)=1$ if $r>0$ and $\theta(r)=0$ if $r<0$. Assuming again that

$$R_c(\theta',\phi')=R_c(1+\sum_{\lambda\mu}\alpha_{\lambda\mu}Y_{\lambda\mu}(\theta',\phi')), \quad (9)$$

inserting (8) with (9) into (7) and then using (6), V_{Coul} is expressed to second order in $\sum_{\lambda\mu}\alpha_{\lambda\mu}Y_{\lambda\mu}$ as

$$V_{\text{Coul}}=(ZZ'\epsilon^2/2R_c)[3-(r^2/R_c^2)]\theta(R_c-r)$$
$$+(ZZ'\epsilon^2/r)\theta(r-R_c)$$
$$+\sum_{\lambda\mu}(3ZZ'\epsilon^2/(2\lambda+1))[r^{\lambda}R_c^{-(\lambda+1)}\theta(R_c-r)$$
$$+R_c^{\lambda}r^{-(\lambda+1)}\theta(r-R_c)](\alpha_{\lambda\mu}Y_{\lambda\mu})$$
$$+\sum_{\lambda\mu}(3ZZ'\epsilon^2/(2\lambda+1))[(1-\lambda)r^{\lambda}R_c^{-(\lambda+1)}\theta(R_c-r)$$
$$+(\lambda+2)R_c^{\lambda}r^{-(\lambda+1)}\theta(r-R_c)]$$
$$\cdot\sum_{\lambda'\lambda''}(\hat{\lambda}'\hat{\lambda}''/(4\pi)^{\frac{1}{2}}\hat{\lambda})(\lambda'\lambda''00\mid\lambda0)\sum_{\mu}(\alpha_{\lambda'}\otimes\alpha_{\lambda''})_{\lambda\mu}Y_{\lambda\mu}. \quad (10)$$

From (5), (6), and (10) we now have

$$V(r,\theta,\phi)=V_{\text{diag}}+V_{\text{coupl}}^{(v)}, \quad (11)$$

where

$$V_{\text{diag}}=-(V+iW)(1+e)^{-1}-4iW_D\bar{e}(1+\bar{e})^{-2}$$
$$-V_{SO}(\lambda_\pi^2/ar)(\boldsymbol{\sigma}\cdot\mathbf{l})e(1+e)^{-2}$$
$$+\frac{ZZ'\epsilon^2}{2R_c}\left(3-\frac{r^2}{R_c^2}\right)\theta(R_c-r)+\frac{ZZ'\epsilon^2}{r}\theta(r-R_c), \quad (12)$$

and

$$V_{\text{coupl}}^{(v)}=\sum_{\lambda\mu}v_{cp;\lambda}^{(1)(v)}(r)\alpha_{\lambda\mu}Y_{\lambda\mu}$$
$$+\sum_{\lambda\lambda_1\lambda_2}V_{cp;\lambda}^{(2)(v)}(r)(\hat{\lambda}_1\hat{\lambda}_2/(4\pi)^{\frac{1}{2}}\hat{\lambda})(\lambda_1\lambda_200\mid\lambda0)$$
$$\cdot\sum_{\mu}(\alpha_{\lambda_1}\otimes\alpha_{\lambda_2})_{\lambda\mu}Y_{\lambda\mu}, \quad (13)$$

with

$$v_{cp;\lambda}^{(1)(v)}(r)=-\{(V+iW)(R_0/a)e(1+e)^{-2}$$
$$-4iW_D(\bar{R}_0/\bar{a})\bar{e}(1-\bar{e})(1+\bar{e})^{-3}\}$$
$$+(3ZZ'\epsilon^2/(2\lambda+1))\{r^{\lambda}R_c^{-(\lambda+1)}\theta(R_c-r)$$
$$+R_c^{\lambda}r^{-(\lambda+1)}\theta(r-R_c)\}, \quad (13.1)$$

and

$$v_{cp;\lambda}^{(2)(v)}(r)=(V+iW)(R_0^2/2a^2)e(1-e)(1+e)^{-3}$$
$$-4iW_D(\bar{R}_0^2/2\bar{a}^2)\bar{e}(1-4\bar{e}+\bar{e}^2)(1+\bar{e})^{-4}$$
$$+(3ZZ'\epsilon^2/(2\lambda+1))\{(1-\lambda)r^{\lambda}R_c^{-(\lambda+1)}\theta(R_c-r)$$
$$+(\lambda+2)R_c^{\lambda}r^{-(\lambda+1)}\theta(r-R_c)\}. \quad (13.2)$$

The potential V_{diag} is diagonal with respect to the total spin j of the projectile and the eigenspin I of the target nucleus, and is nothing but the usual optical-model potential.[16] On the other hand, $V_{\text{coupl}}^{(v)}$ gives the coupling potential between channels which have different j and I, the superfix (v) meaning that we are considering vibrational nuclei as targets.

(ii) For a rotational nucleus, one should use (3) in (1). If the resulting potential is again expanded in powers of $\sum_\lambda\beta_\lambda Y_{\lambda0}(\theta')$, one gets exactly the same expression as in (i), namely Eqs. (11) through (13), except that $\alpha_{\lambda\mu}$ and $Y_{\lambda\mu}(\theta,\phi)$, are replaced, respectively, by β_λ and $Y_{\lambda0}(\theta')=\sum_\mu D_{\mu0}^{\lambda}(\theta_i)Y_{\lambda\mu}(\theta,\phi)$. Here $D_{\mu0}^{\lambda}(\theta_i)$ is a rotation matrix[18] and θ_i stands for the Euler angles between the body-fixed and the space-fixed coordinates. As was noticed by Buck,[7] while the first term of (13) in the vibrational nucleus has vanishing diagonal elements, the corresponding term in the rotational nucleus has nonvanishing diagonal elements, and this difference can give rise to a large difference in the calculated differential cross sections, in some cases.

This is certainly an important remark. Nevertheless, as was discussed by Chase *et al.*,[3] and is also exemplified

[17] R. H. Bassel, R. M. Drisko, and G. R. Satchler, Oak Ridge National Laboratory Report ORNL-3240, 1962 (unpublished).

[18] See, e.g., D. M. Brink and G. R. Satchler, *Angular Momentum* (Oxford University Press, Oxford, 1962).

in Sec. VI, the approximation of expanding the potential in powers of $\sum_\lambda \beta_\lambda Y_{\lambda 0}(\theta')$ and then retaining a few of its leading terms turns out to be rather poor when β_λ is as large as, say, 0.3, as is the case in many actual deformed nuclei. Since the parameter β_λ is a c number, contrary to $\alpha_{\lambda\mu}$ which must be treated as a q-number operator, one can expand Eq. (1) with (3), not in powers of $\sum_\lambda \beta_\lambda Y_{\lambda 0}(\theta')$, but in terms of the Legendre polynomials P_λ (cos θ'), or rather in terms of $Y_{\lambda 0}(\theta')=(2\lambda+1/4\pi)^{\frac{1}{2}}P_\lambda$ (cos θ'), and then replace $Y_{\lambda 0}(\theta')$ by $\sum_\mu D_{\mu 0}^{\lambda}(\theta_i)\, Y_{\lambda\mu}(\theta, \phi)$. If this is done, the radial function which appears as the coefficient of $Y_{\lambda 0}(\theta')$ for each given λ is the sum of the contributions of an infinite number of terms in the power-series expansion in $\sum_\lambda \beta_{\lambda'} Y_{\lambda' 0}(\theta')$. Therefore the Legendre polynomial expansion can be a much better approximation than the power series expansion. (It is unfortunate that a similar procedure is very hard to make for vibrational nuclei.)

The calculation of the Legendre polynomial expansion is straightforward, and it is enough simply to give the final result. We again have

$$V(r, \theta, \phi)=V_{\text{diag}}+V_{\text{coupl}}{}^{(r)}, \tag{14}$$

where $V_{\text{coupl}}{}^{(r)}$ is given by

$$V_{\text{coupl}}{}^{(r)}=\sum_{\lambda\mu(\lambda\neq 0)} v_{cp}{}^{(\lambda)(r)}(r)\, D_{\mu 0}{}^{\lambda} Y_{\lambda\mu}(\theta, \phi) \tag{15}$$

with[13]

$$v_{cp}{}^{(\lambda)(r)}(r)$$

$$=4\pi\int_0^1\Bigg\{\frac{-(V+iW)}{1+\exp\,[[r-R_0(1+\sum_{\lambda'}\beta_{\lambda'}Y_{\lambda' 0}(\theta'))]/a]}$$

$$+\frac{-4iW_D\exp\,[[r-\bar{R}_0(1+\sum_{\lambda'}\beta_{\lambda'}Y_{\lambda' 0}(\theta'))]/\bar{a}]}{\{1+\exp\,[[r-\bar{R}_0(1+\sum_{\lambda'}\beta_{\lambda'}Y_{\lambda' 0}(\theta'))]/\bar{a}]\}^2}\Bigg\}$$

$$\times Y_{\lambda 0}(\theta')\, d\,(\cos\theta'). \tag{16}$$

On the other hand, V_{diag} is the same as in (12), except that the first two terms in it are to be replaced by $(4\pi)^{-\frac{1}{2}}$ times $v_{cp}{}^{(0)(r)}(r)$ of (16). In (15) with (16) we gave only the nuclear part of the coupling potential. For the Coulomb part perhaps the power-series expansion is a sufficiently good approximation. Therefore, the Coulomb interaction for a deformed nucleus can be taken into account by adding to (15) the Coulomb part of (13) after replacing $\alpha_{\lambda\mu}Y_{\lambda\mu}$ by $\beta_\lambda D_{\mu 0}{}^{\lambda} Y_{\lambda\mu}$.

III. THE COUPLED EQUATIONS

Let us assume that there are N_s states in the target nucleus which are coupled strongly (directly or indirectly) to the ground state by the V_{coupl} given in (13) or (15). We label these states with $n=1$ to N_s, $n=1$ meaning the ground state, and we let the spin, parity, and energy of the nth state be I_n, π_n, and ω_n, respectively. Then if the energy of the incident particle (in the center-of-mass system) is E_1 the energy of the particle which leaves the target in its nth state has energy $E_n=E_1-\omega_n$.

In a channel corresponding to the nth state of the target consider a partial wave of a projectile of a spin s that has orbital angular momentum l_n and total angular momentum $j_n(=\mathbf{l}_n+\mathbf{s})$. Couple this j_n to I_n vectorially and define an angular momentum J of the whole system together with a parity operator Π also of the whole system:

$$J=\mathbf{j}_n+\mathbf{I}_n \quad \text{and} \quad \Pi=\pi_n(-)^{l_n}. \tag{17}$$

With the interaction (13) or (15), it is easy to see that none of l_n, j_n, I_n, π_n or $(-)^{l_n}$ is a good quantum number, but J as well as Π is good. In other words, several partial waves whose l_n and j_n satisfy (17) for a given set of J and Π are coupled together through (13) or (15) to form a set of coupled differential equations. We denote the number of such a set of $(l_n j_n)$ by $n_c{}^{(n)}$ and call its maximum possible number as $N_c{}^{(n)}$. For a given value of I_n the value of $N_c{}^{(n)}$ is as follows:

$$\begin{aligned}
N_c{}^{(n)}&=I_n+1 && \text{if } s=0 \text{ and } I_n \text{ is an integer,}\\
&=I_n+\tfrac{1}{2} && \text{if } s=0 \text{ and } I_n \text{ is a half-integer,}\\
N_c{}^{(n)}&=2I_n+1 && \text{if } s=\tfrac{1}{2}, \text{ all } I_n,\\
N_c{}^{(n)}&=3I_n+2 && \text{if } s=1 \text{ and } I_n \text{ is an integer,}\\
&=3I_n+\tfrac{3}{2} && \text{if } s=1 \text{ and } I_n \text{ is a half-integer.}
\end{aligned} \tag{18}$$

Corresponding to $n_c{}^{(n)}$ and $N_c{}^{(n)}$ we define

$$n_c=\sum_{n=1}^{N_s} n_c{}^{(n)}, \tag{19}$$

and

$$N_c=\sum_{n=1}^{N_s} N_c{}^{(n)}, \tag{20}$$

which give, respectively, the total number of the coupled partial waves $(l_n j_n)$ for a given J and Π, and its maximum possible value.

The terminology to be used is as follows: If we say a "partial-wave channel," it means a channel corresponding to a particular set of values of l_n and j_n. On the other hand if we say a "nth state channel", it means $n_c{}^{(n)}$ sets of values of $(l_n j_n)$, as a whole.

In the actual numerical calculations the values of J are to be varied for each Π from its minimum value $J_{\min}$, which is equal to 0 or $\frac{1}{2}$ depending, respectively, whether I_n+s is an integer or a half-integer, to its maximum value $J_{\max}$, which may be taken as equal to $I_1+j_{\max}$, where $j_{\max}$ is the maximum value of j_1 of the partial wave that gives a non-negligible contribution to the (elastic) scattering.

We now introduce the Hamiltonian

$$H=T+H_t+V(r, \theta, \phi)=T+H_t+V_{\text{diag}}+V_{\text{coupl}}, \tag{21}$$

where T is the kinetic energy of the incident particle and H_t is the Hamiltonian for the internal motion of the target nucleus. The Schrödinger equation can then be written as

$$H\Psi = E_1\Psi, \tag{22}$$

where the total wave function Ψ may be written as

$$\Psi = r^{-1}\sum_{Jnl_nj_n} R_{Jnl_nj_n}(r)\,(\mathcal{Y}_{l_nj_n}\otimes\Phi_{I_n})_{JM}$$
$$= r^{-1}\sum_{Jnl_nj_n} R_{Jnl_nj_n}(r)\sum_{m_jM_n}(j_nI_nm_jM_n \mid JM)\,\mathcal{Y}_{l_nj_nm_j}\Phi_{I_nM_n}. \tag{23}$$

In (23)

$$\mathcal{Y}_{l_nj_nm_j} = \sum_{m_lm_s}(lsm_lm_s \mid jm_j)\,i^l Y_{l_nm_l}\chi_{sm_s},$$

χ_{sm_s} being the spin wave function of the projectile, while $\Phi_{I_nM_n}$ is the wave function of the target nucleus in its nth state. By definition we have

$$H_t\Phi_{I_nM_n} = \omega_n\Phi_{I_nM_n}. \tag{24}$$

Inserting (21) and (23) into (22), multiplying it by $(\mathcal{Y}_{l_nj_n}\otimes\Phi_{I_n})_{JM}{}^*$ from the left, and integrating over all the coordinates except the radial variable r, and finally dividing by E_n, one gets the following equation:

$$\left(\frac{d^2}{d\rho_n{}^2}-\frac{l_n(l_n+1)}{\rho_n{}^2}-\frac{1}{E_n}V_{\text{diag}}+1\right)R_{Jnl_nj_n}(r) = E_n{}^{-1}\sum_{n'l_n'j_n'}\langle(\mathcal{Y}_{l_nj_n}\otimes\Phi_{I_n})_{JM} \mid V_{\text{coupl}} \mid (\mathcal{Y}_{l_n'j_n'}\otimes\Phi_{I_n'})_{JM}\rangle R_{Jn'l_nj_n'}(r)$$
$$(\rho_n = k_nr;\quad k_n \text{ is the wave number}). \tag{25}$$

Equation (25) represents a set of n_c coupled equations.

Equation (25) is quite general and holds irrespective of the nature of the projectile or the target nucleus. Assumptions about the nuclear structure only affect the matrix elements that appear on the right-hand side of that equation, and the evaluation of that matrix element is the most crucial part of the whole calculation. However, the coupling term V_{coupl} can still be written in a general form as

$$V_{\text{coupl}} = \sum_{t,\lambda} v_\lambda{}^{(t)}(r)\,(Q_\lambda{}^{(t)}\cdot Y_\lambda), \tag{26}$$

where the superscript t conveniently discriminates terms of different character but the same tensorial rank λ, and $Q_\lambda{}^{(t)}$ means an operator which operates only on the coordinates of the target nucleus. The calculation of the matrix element is straightforward and the result is given by

$$\langle(\mathcal{Y}_{lj}\otimes\Phi_I)_{JM} \mid V_{\text{coupl}} \mid (\mathcal{Y}_{l'j'}\otimes\Phi_{I'})_{JM}\rangle$$
$$\equiv \langle ljI \mid V_{\text{coupl}} \mid l'j'I'\rangle$$
$$= \sum_{t,\lambda} v_\lambda{}^{(t)}(r)\,\langle I \mid\mid Q_\lambda{}^{(t)} \mid\mid I'\rangle A(ljI, l'j'I', \lambda Js), \tag{27}$$

with

$$A(ljI, l'j'I'; \lambda Js) = (4\pi)^{-\frac{1}{2}}(-)^{J-s-I'+l+l'+\frac{1}{2}(l'-l)}$$
$$\cdot\hat{l}\hat{l}'\hat{j}\hat{j}'(l'00 \mid \lambda 0)\,W(jIj'I'; J\lambda)\,W(ljl'j'; s\lambda). \tag{28}$$

The factor $A(ljI, l'j'I'; \lambda Js)$ in (27) is completely geometrical. When $s=\frac{1}{2}$ it reduces to

$$A(ljI, l'j'I'; \lambda J\tfrac{1}{2}) = (4\pi)^{-\frac{1}{2}}(-)^{J-\frac{1}{2}-I'+j+j'+\frac{1}{2}(l'-l)}$$
$$\cdot\hat{j}\hat{j}'(jj'-\tfrac{1}{2}\tfrac{1}{2} \mid \lambda 0)\,W(jIj'I'; J\lambda), \tag{29.1}$$

while if $s=0$ it becomes

$$A(ljI, l'j'I'; \lambda J0) = (4\pi)^{-\frac{1}{2}}(-)^{J-I'+l+l'+\frac{1}{2}(l'-l)}$$
$$\cdot\hat{l}\hat{l}'(l'00 \mid \lambda 0)\,W(lIl'I'; J\lambda)\,\delta_{lj}\,\delta_{l'j'}. \tag{29.2}$$

The reduced matrix element $\langle I \mid\mid Q_\lambda{}^{(t)} \mid\mid I'\rangle$ appearing in (27) is defined by

$$\langle IM_I \mid Q_{\lambda\mu}{}^{(t)} \mid I'M_I'\rangle = \langle I \mid\mid Q_\lambda{}^{(t)} \mid\mid I'\rangle\hat{I}^{-1}(I'\lambda M_I'\mu \mid IM_I), \tag{30}$$

and contains all the dynamics involved in the problem. Here I stands for all the quantum numbers needed in specifying the state that is simply written as $\mid I\rangle$.

We now give the explicit form of the reduced matrix elements $\langle I \mid\mid Q_\lambda{}^{(t)} \mid\mid I'\rangle$ for various interesting cases.[18a]

A. Vibrational Nucleus (Even Mass)

Comparing (26) with (13) one can write

$$Q_{\lambda\mu}{}^{(1)} = \alpha_{\lambda\mu}, \tag{31.1}$$

$$Q_{\lambda\mu}{}^{(2)} = \sum_{\lambda_1\lambda_2}(\hat{\lambda}_1\hat{\lambda}_2/(4\pi)^{\frac{1}{2}}\hat{\lambda})(\lambda_1\lambda_200 \mid \lambda 0)\,(\alpha_{\lambda_1}\otimes\alpha_{\lambda_2})_{\lambda\mu}. \tag{31.2}$$

Following Bohr[19] we introduce the creation and annihilation operators $b_{\lambda\mu}$ and $b_{\lambda\mu}{}^*$, and express the operator $\alpha_{\lambda\mu}$ as

$$\alpha_{\lambda\mu} = \beta_\lambda\hat{\lambda}^{-1}(b_{\lambda\mu} + (-)^\mu b_{\lambda-\mu}{}^*). \tag{32}$$

Using this $b_{\lambda\mu}{}^*$, and denoting the no-phonon (ground) state by $\mid 0\rangle$, the wave functions of various vibrational states (with spins I and its projection M) are written as follows.

(a) One-phonon state:

$$\mid 1; IM\rangle = b_{IM}{}^* \mid 0\rangle. \tag{33}$$

(b) Two-phonon states (one phonon of multipolarity λ_1 and the other with multipolarity λ_2):

$$\mid 2; IM\rangle = (1+\delta_{\lambda_1\lambda_2})^{-\frac{1}{2}}(b_{\lambda_1}{}^*\otimes b_{\lambda_2}{}^*)_{IM} \mid 0\rangle. \tag{34}$$

[18a] The reduced electric transition probability is related to this reduced matrix element by $B(E\lambda; I\to I') = (\hat{I}'/\hat{I})^2B(E\lambda; I'\to I) = |\langle I \mid\mid Q_\lambda{}^{(t)} \mid\mid I'\rangle|^2/\hat{I}^2$.

[19] A. Bohr, Kgl. Danske Videnskab. Selskab, Mat. Fys. Medd. **26**, No. 14 (1952).

TABLE I. Values of the quantities needed in describing the coupling of the one- and two-phonon states to the three-phonon states.

A. Fractional parentage coefficients $N_I^{(I')}$ of Eq. (35).

	I'				
I	0	2	3	4	6
0	0	$(7/90)^{\frac{1}{2}}$	0	0	0
2	$(1/6)^{\frac{1}{2}}$	$(2/63)^{\frac{1}{2}}$	$(5/42)^{\frac{1}{2}}$	$(11/126)^{\frac{1}{2}}$	0
4	0	$(2/35)^{\frac{1}{2}}$	$-(1/21)^{\frac{1}{2}}$	$(5/63)^{\frac{1}{2}}$	$(1/6)^{\frac{1}{2}}$

B. Quantities $B_{II'}$ of Eq. (36-3).

	I'				
I	0	2	3	4	6
0	0	$(14)^{\frac{1}{2}}$	0	0	0
2	$(6)^{\frac{1}{2}}$	$(40/7)^{\frac{1}{2}}$	$-(30)^{\frac{1}{2}}$	$(198/7)^{\frac{1}{2}}$	0
4	0	$(72/7)^{\frac{1}{2}}$	$(12)^{\frac{1}{2}}$	$(180/7)^{\frac{1}{2}}$	$(78)^{\frac{1}{2}}$

C. Quantities $C_{I\lambda}$ of Eq. (37-2).

	I				
λ	0	2	3	4	6
0	0	$(7/5)^{\frac{1}{2}}$	0	0	0
2	$-(6/35)^{\frac{1}{2}}$	$-(8/49)^{\frac{1}{2}}$	$(2/21)^{\frac{1}{2}}$	$-(198/245)^{\frac{1}{2}}$	0
4	0	$(72/245)^{\frac{1}{2}}$	$(4/105)^{\frac{1}{2}}$	6/7	$(78/35)^{\frac{1}{2}}$

(c) Three-quadrupole-phonon states:

$$|\,3;IM\rangle=\sum_{I'}N_I^{(I')}((b_2^*\otimes b_2^*)_{I'}\otimes b_2^*)_{IM}\,|\,0\rangle, \quad (35)$$

where the values of the fractional parentage coefficients $N_I^{(I')}$ are given in Table I(A).

Using (31) for the operators $Q_{\lambda\mu}^{(1)}$ and $Q_{\lambda\mu}^{(2)}$, and (33), (34), and (35) for the wave functions, the evaluation of the matrix elements $\langle I\,||\,Q_\lambda^{(i)}\,||\,I'\rangle$ of (27) is straightforward and the results for those which are used in the calculation of Secs. VI and VII are summarized as follows.

(*i*) *Operators linear in* α_λ

(a′) Ground state↔one-phonon states (arbitrary λ):

$$\langle 0;0\,||\,Q_\lambda^{(1)}\,||\,1;I\rangle=\delta_{\lambda I}(-)^I\beta_\lambda. \quad (36.1)$$

(b′) One-quadrupole-phonon state↔two-quadrupole-phonon states:

$$\langle 1;2\,||\,Q_2^{(1)}\,||\,2;I\rangle=\beta_2[2(2I+1)/5]^{\frac{1}{2}}. \quad (36.2)$$

(c′) Two-quadrupole-phonon states↔three-quadrupole-phonon states:

$$\langle 2;I\,||\,Q_2^{(1)}\,||\,3;I'\rangle=(\beta_2/10^{\frac{1}{2}})\sum_{I''}N_I^{(I'')}(2\delta_{II''}(-)^{I+I'}\hat{I}'$$
$$+4\hat{I}\hat{I}'\hat{I}''W(222I';I''I))$$
$$\equiv(\beta_2/10^{\frac{1}{2}})B_{II'}, \quad (36.3)$$

where the values of the quantities $B_{II'}$ are given in Table I(B).

(d′) One-octupole-phonon state↔quadrupole-octupole-two-phonon states:

$$\langle 1;3\,||\,Q_2^{(1)}\,||\,(2\otimes 3);I\rangle=\beta_2[(2I+1)/5]^{\frac{1}{2}}. \quad (36.4)$$

(e′) One-quadrupole-phonon state↔quadrupole-octupole-two-phonon states:

$$\langle 1;2\,||\,Q_3^{(1)}\,||\,(2\otimes 3);I\rangle=\beta_3(-)^I[(2I+1)/7]^{\frac{1}{2}}. \quad (36.5)$$

(*ii*) *Operators quadratic in* α_λ

(a″) Ground state↔two-quadrupole-phonon states:

$$\langle 0;0\,||\,Q_\lambda^{(2)}(\lambda_1=\lambda_2=2)\,||\,2;I\rangle$$
$$=\beta_2^2\,\delta_{I\lambda}(2200\,|\,I0)/(2\pi)^{\frac{1}{2}}. \quad (37.1)$$

(b″) One-quadrupole-phonon↔three-quadrupole-phonon state:

$$\langle 1;2\,||\,Q_\lambda^{(2)}(\lambda_1=\lambda_2=2)\,||\,3;I\rangle$$
$$=\beta_2^2(2200\,|\,\lambda 0)\sum_{I''}N_I^{(I'')}$$
$$\cdot(2\,\delta_{I''\lambda}\hat{I}\hat{\lambda}^{-1}+4\hat{I}\hat{I}''W(222I;I''\lambda))/(4\pi)^{\frac{1}{2}}$$
$$\equiv\beta_2^2C_{I\lambda}/(2\pi)^{\frac{1}{2}}, \quad (37.2)$$

where the values of the quantities $C_{I\lambda}$ are given in Table I(C).

(c″) Ground state↔quadrupole-octupole-two-phonon states:

$$\langle 0;0\,||\,Q_\lambda^{(2)}(\lambda_1=2,\lambda_2=3)\,||\,(2\otimes 3);I\rangle$$
$$=\beta_2\beta_3\,\delta_{\lambda I}(2300\,|\,I0)(-)^{I+1}/(4\pi)^{\frac{1}{2}}. \quad (37.3)$$

(d″) One-quadrupole-phonon state↔one-octupole

phonon state:

$$\langle 1;2 \,||\, Q_\lambda^{(2)}(\lambda_1=2,\lambda_2=3) \,||\, 1;3\rangle = \beta_2\beta_3(2300 \mid \lambda 0)/(4\pi)^{\frac{1}{2}}. \quad (37.4)$$

All of (36) and (37) are nondiagonal elements. Since

$$\langle I \,||\, Q_\lambda^{(t)} \,||\, I'\rangle = (-)^{I-I'+\lambda}\langle I' \,||\, Q_\lambda^{(t)} \,||\, I\rangle \quad (38)$$

holds, the matrix $||\, \langle I \,||\, Q_\lambda^{(t)} \,||\, I'\rangle \,||$ which we refer to as the B matrix in the following is not Hermitian. Since, however, the A matrix (28) has the same property as (38) with respect to the interchange of its row and column, the whole matrix (27) is Hermitian, as it should be.

When $\lambda_1=\lambda_2$ in (31.2), it contributes nonvanishing diagonal elements. We give here only the expressions for $\lambda_1=\lambda_2=2$ for zero, one- and two-quadrupole-phonon states.

(a‴) Ground state:

$$\langle 0;0 \,||\, Q_\lambda^{(2)}(\lambda_1=\lambda_2=2) \,||\, 0;0\rangle = \beta_2^2\,\delta_{\lambda 0}/(4\pi)^{\frac{1}{2}}. \quad (39.1)$$

(b‴) One-quadrupole-phonon state:

$$\langle 1;2 \,||\, Q_\lambda^{(2)}(\lambda_1=\lambda_2=2) \,||\, 1;2\rangle = \beta_2^2(2200 \mid \lambda 0)\,(2+5\,\delta_{\lambda 0})/(4\pi)^{\frac{1}{2}}. \quad (39.2)$$

(c‴) Two-quadrupole-phonon states:

$$\langle 2;I \,||\, Q_\lambda^{(2)}(\lambda_1=\lambda_2=2) \,||\, 2;I'\rangle = \beta_2^2(4\pi)^{-\frac{1}{2}}\lambda^{-1}(2200 \mid \lambda 0) \times\{5^{\frac{1}{2}}\hat{I}\,\delta_{\lambda 0}\,\delta_{II'}+4\hat{I}\hat{I}'\hat{\lambda}W(2I2I';2\lambda)\}. \quad (39.3)$$

B. Rotational Nuclei

We consider here only the excitation of the states which belong to the ground rotational band. Then the expression for the coupling matrix becomes extremely simple:

$$\langle ljI \mid V_{\text{coupl}} \mid l'j'I'\rangle_{JM} = \sum_\lambda v_{cp}^{(\lambda)(r)}(r)B_\lambda(I,I')A(ljI,l'j'I';\lambda Js), \quad (40)$$

where

$$B_\lambda(I,I')=\hat{I}'(I'\lambda K0 \mid IK). \quad (41)$$

If excitations of the β and/or γ vibrations are also considered, the expression for the matrix $B_\lambda(I,I')$ becomes more involved [cf. Sec. VII(B3)].

IV. SCATTERING MATRICES AND CROSS SECTIONS

We are now ready to solve the coupled equation (25) for the radial wave functions $R_{Jnlj}(r)$. If the solution thus obtained is matched at an appropriate matching radius, R_m, to its corresponding asymptotic solution, the scattering coefficient or the S matrix is obtained.

In order to write down the asymptotic solution explicitly, we first assume that initially both the projectile and the target are in some polarized states (including the unpolarized state as a special case), and that their polarized states are described by the amplitudes $a_{m_s}^{(i)}$ and $b_{M_1}^{(i')}$, respectively. Here the superscripts (i) and (i') specify different spin ensembles when more than one ensemble is needed for the description of the polarized state. It is understood that amplitudes for projectiles or targets which belong to different ensembles do not interfere, but the amplitudes for those which belong to the same ensemble but have different magnetic quantum numbers do interfere with each other.

As will be seen at the end of this section, the expressions for $a_{m_s}^{(i)}$ and $b_{M_1}^{(i')}$ become very simple if only unpolarized projectiles and unpolarized targets were considered. In such a case the expressions for the cross sections which are given below are also very much simplified, being reduced to those that were already given in literatures,[2–4,7,15] and we could thus dispense with the present section completely. In order to make the present paper self-contained, however, and to make it clear how the amplitudes $a_{m_s}^{(i)}$ and $b_{M_1}^{(i')}$ play their role when either or both of the projectiles and the targets are indeed polarized, it is desirable to give all the following expressions explicitly.

A. Shape Scattering Cross Sections and Polarizations

Using the amplitudes $a_{m_s}^{(i)}$ and $b_{M_1}^{(i')}$, the asymptotic form of the wave function may be written as

$$\Psi_{\text{asym}}=[(4\pi)^{\frac{1}{2}}/rk_1(v_1)^{\frac{1}{2}}]\sum_{(ii')m_sM_1} a_{m_s}^{(i)}b_{M_1}^{(i')} \cdot\sum_{ljJM}(ls0m_s \mid jm_s)\,(jI_1m_sM_1 \mid JM) \cdot\sum_{nl'j'}[\hat{l}\exp(i\sigma_l^{(1)})\,\delta_{n1}\,\delta_{l'l}\,\delta_{j'j}F_l^{(1)} +(k_1/k_n)^{\frac{1}{2}}\hat{l}'\exp(i\sigma_{l'}^{(n)}) \cdot C_{lj;nl'j'}^{J}(G_{l'}^{(n)}+iF_{l'}^{(n)})](\mathcal{Y}_{l'j'}\otimes\Phi_{I_n})_{JM}. \quad (42)$$

In (42) $F_l^{(n)}$ and $G_l^{(n)}$ are, respectively, regular and irregular Coulomb wave functions (at $r=R_m$), specified with the orbital angular momentum l and the energy E_n, as well as the parameter $\eta_n=mZZ'\epsilon^2/\hbar^2k_n$ (m is the reduced mass of the projectile). $\sigma_l^{(n)}$ is the corresponding Coulomb phase shift.

All the expressions in the present section including Eq. (42) are given for charged projectiles. It is easy, however, to get the corresponding expressions appropriate for uncharged projectiles by putting equal to zero the parameter η_n, the Coulomb phase shift $\sigma_l^{(n)}$ and the Rutherford amplitude $f_c(\theta)$ that appear below. We should further replace $F_l^{(n)}$ and $G_l^{(n)}$, respectively, by $\rho_n j_l^{(n)}$ and $\rho_n n_l^{(n)}$, where $j_l^{(n)}$ and $n_l^{(n)}$ are spherical Bessel and Neuman functions, respectively, while $\rho_n=k_nR_m$.

Comparing the forms of (23) and (42) we can immediately write down the matching equation and the scattering coefficients $C_{lj;nl'j'}{}^{J}$ are obtained by solving these equations.

In deriving the expression for the scattering cross section from (42), we first note that the first term of (42) is just the incident wave Ψ_{inc}, which is the sum of the (Coulomb distorted) plane wave and the Coulomb scattered wave;

$$\Psi_{\text{inc}}=[1/(v_1)^{\frac{1}{2}}]\{\exp[i(k_1z-\eta_1\ln(2k_1\mid r-z\mid))]\cdot\{1-[\eta_1^2/ik_1(r-z)]\}+r^{-1}f_c(\theta)\cdot\exp[i(k_1r-\eta_1\ln(2k_1r))]\}\cdot\sum_{(ii')m_sM_1}a_{m_s}{}^{(i)}b_{M_1}{}^{(i')}\chi_{sm_s}\Phi_{I_1M_1},\quad(43)$$

where $f_c(\theta)$ is the Rutherford scattering amplitude.

Corresponding to (43) we rewrite the second term of (42) by noting that asymptotically

$$G_l{}^{(n)}\underset{r\to\infty}{\longrightarrow}\cos(\Sigma_l{}^{(n)}),\qquad F_l{}^{(n)}\underset{r\to\infty}{\longrightarrow}\sin(\Sigma_l{}^{(n)}),\quad(44)$$

with

$$\Sigma_l{}^{(n)}=k_nr-\eta_n\ln(2k_nr)-(l\pi/2)+\sigma_l{}^{(n)}.\quad(45)$$

Adding the second terms of (42) and (43), the wave function for the scattered wave, Ψ_{scatt}, is now given as

$$\Psi_{\text{scatt}}=\sum_n\frac{\exp[i(k_nr-\ln(2k_nr)]}{r(v_n)^{\frac{1}{2}}}\sum_{(ii')m_sM_1}a_{m_s}{}^{(i)}b_{M_1}{}^{(i')}\cdot\{f_c(\theta)\,\delta_{n1}\chi_{sm_s}\Phi_{I_1M_1}+\sum_{ljl'j'J}(4\pi/k_n^2)^{\frac{1}{2}}\hat{l}'\cdot\exp(2i\sigma_{l'}{}^{(n)})C_{lj;nl'j'}{}^{J}(ls0m_s\mid jm_s)\cdot(jI_1m_sM_1\mid JM)(\mathcal{Y}_{l'j'}\otimes\Phi_{I_n})_{JM}\}.\quad(46)$$

The shape scattering differential cross sections $\sigma_n{}^{(s)}(\theta,\phi)$, which leaves the target in its nth state is given as the absolute square of the second sum of (46). Therefore we get

$$\sigma_n{}^{(s)}(\theta,\phi)=\sum_{ii'm_s'M_n}\Big|\sum_{m_sM_1}a_{m_s}{}^{(i)}b_{M_1}{}^{(i')}\{f_c(\theta)\,\delta_{n1}\,\delta_{m_s'm_s}\,\delta_{M_nM_1}+\sum_{ljl'j'Jm_l'm_j'}(4\pi/k_n^2)^{\frac{1}{2}}\hat{l}'\cdot\exp(2i\sigma_{l'}{}^{(n)})C_{lj;nl'j'}{}^{J}(ls0m_s\mid jm_s)\cdot(jI_1m_sM_1\mid JM)\cdot(l'sm_l'm_s'\mid j'm_j')(j'I_nm_j'M_n\mid JM)Y_{l'm_l'}(\theta,\phi)\}\Big|^2.\quad(47)$$

Note that $\sigma_n{}^{(s)}(\theta,\phi)$ depends in general on the azimuthal angle ϕ.

If the square of each term of (47) is actually taken and summation over the magnetic quantum numbers is performed, $\sigma_n{}^{(s)}(\theta,\phi)$ can be expressed in terms of the Racah and Z coefficients.[20] For the machine calculation, however, it is found that the form of (47) is more suitable, and thus we leave it as it is.[21]

In order to express (47) in a more compact form, we shall introduce an amplitude $X_{m_sM_1;m_s'M_n}(\theta,\phi)$ defined as

$$X_{m_sM_1;m_s'M_n}(\theta,\phi)=f_c(\theta)\,\delta_{n1}\,\delta_{m_s'm_s}\,\delta_{M_nM_1}+\sum_{ljl'j'Jm_l'm_j'M}(4\pi/k_n^2)^{\frac{1}{2}}\hat{l}'\exp(2i\sigma_{l'}{}^{(n)})\cdot C_{lj;nl'j'}{}^{J}(lsom_s\mid jm_s)(jI_1m_sM_1\mid JM)\cdot(l'sm_l'm_s'\mid j'm_j')(j'I_nm_j'M_n\mid JM)Y_{l'm_l'}(\theta,\phi).\quad(48)$$

Then, of course, (47) is reduced to

$$\sigma_n{}^{(s)}(\theta,\phi)=\sum_{ii_1m_s'M_n}\Big|\sum_{m_sM_1}X_{m_sM_1;m_s'M_n}(\theta,\phi)a_{m_s}{}^{(i)}b_{M_1}{}^{(i')}\Big|^2.\quad(49)$$

The amplitude (48) allows us to write down the expression for the polarization also in a compact form. The (vector) polarization $P_{\mathbf{n}}(\theta,\phi)$, parallel to a given unit vector $\mathbf{n}$, of the particle scattered in the direction specified by the polar angles (θ,ϕ) and leaving the target in its nth state, is defined as the expectation value of the operator $(\boldsymbol{\sigma}\cdot\mathbf{n})$ with respect to the scattered amplitude, i.e., the second sum of (46), divided by $\sigma_n{}^{(s)}(\theta,\phi)$. We thus have

$$\sigma_n{}^{(s)}(\theta,\phi)P_{\mathbf{n}}(\theta,\phi)=\sum_{ii'}\sum_{(m)}X^*_{m_sM_1,m_s'M_n}(\theta,\phi)X_{\bar{m}_s\bar{M}_1;\bar{m}_s'\bar{M}_n}(\theta,\phi)\cdot\langle m_s'\mid(\boldsymbol{\sigma}\cdot\mathbf{n})\mid\bar{m}_s'\rangle a_{m_s}{}^{(i)*}b_{M_1}{}^{(i')*}a_{\bar{m}_s'}{}^{(i)}b_{\bar{M}_1}{}^{(i')},\quad(50)$$

where $\sum_{(m)}$ means summation over all the magnetic quantum numbers that appear.

B. Total and Reaction Cross Sections

If the $n=1$ part of (42) is written as Ψ_1 and the quantity

$$\frac{\hbar}{2im}\int\left[\Psi_1\frac{\partial\Psi_1{}^{+}}{\partial r}-\Psi_1{}^{+}\frac{\partial\Psi_1}{\partial r}\right]_r r^2\,d\tau\,d\Omega\quad(51)$$

is computed, this is nothing but the reaction cross section σ_r. In (51) $d\tau$ means summation and integration over all the internal coordinates, while $d\Omega$ means inte-

[20] L. C. Biedenharn, J. M. Blatt, and M. E. Rose, Rev. Mod. Phys. **24**, 249 (1952).

[21] In treating the polarized targets and projectiles, it is customary to introduce the statistical tensors rather than the amplitudes a and b as we did here. See, e.g., L. J. B. Goldfarb and D. A. Bromley, Nucl. Phys. **39**, 408 (1962). We believe, however, the use of a and b is much handier particularly when the polarized state of the target is rather complicated, as for example we shall see below in Sec. VIIB. Also, the fact that it is easier for the machine calculation to compute the amplitude first and then to take its square as made in (47), justifies the use of a and b, rather than the statistical tensors.

gration over all the angular variables of the relative motion. If the total shape elastic cross section σ_{el} [the integral of (47) over $d\Omega$] is added to σ_r, the result is the total cross section σ_t (which is to be compared with the experimental total cross section as obtained by the transmission experiment). If the incident particle is charged, σ_{el} and σ_t are both infinity and thus consideration on these cross sections has meaning only when a neutral particle is used as the projectile.

The expressions for σ_t and σ_r become simplified by introducing an amplitude $Z_{m_sM_1,m_s'M_1';l'}$, which is intimately related to the amplitude $X_{m_sM_1;m_s'M_n}(\theta, \phi)$ of (48), and is defined as

$$Z_{m_sM_1,m_s'M_1';l'}=\sum_{ljj'JMm_lm_j'}(lsom_s\mid jm_s)(jI_1m_sM_1\mid JM)\cdot C_{lj;1l'j'}{}^J(l's0m_s'\mid j'm_s')(j'I_1m_s'M_1'\mid JM). \quad (52)$$

Then

$$\sigma_t=(4\pi/k_1^2)\sum_{l'}(2l'+1)\cdot\{\mathrm{Im}\sum_{ii'm_sm_s'M_1M_1'}a_{m_s}{}^{(i)}a_{m_s'}{}^{(i)*}b_{M_1}{}^{(i')}b_{M_1'}{}^{(i')}Z_{m_sM_1,m_s'M_1';l'}\}, \quad (53)$$

and

$$\sigma_r=\sigma_t-(4\pi/k_1^2)\sum_{l'}(2l'+1)\cdot\sum_{ii'j'J}\mid\sum_{m_sM_1}a_{m_s}{}^{(i)}b_{M_1}{}^{(i')}\sum_{lj}(ls0m_s\mid jm_s)(jI_1m_sM_1\mid JM)C_{lj;1l'j'}{}^J\mid^2. \quad (54)$$

Equation (53) is nothing but the optical theorem in our case and the operator Im appearing there means to take the imaginary part of the expression which follows it.

C. Compound Contribution to the Differential Scattering Cross Sections

When the energy of the incident particle is low, one should not compare the prediction of (47) with experiment but should add the contribution of the compound process to (47), and then compare the sum with the experimental differential cross sections.

It is customary to use the Hauser–Feshbach (HF) formalism[22] in evaluating the compound cross section. Although it is known that this formalism can give rise to some error,[23,24] we follow it since we do not know any other way to handle the problem simply enough.

As is well known, the original HF cross section was given as a function of the penetrabilities $T_l^{(n)}$ for various channels n and the orbital angular momentum l. In computing $T_l^{(n)}$, the scattering coefficient, say $C_l^{(n)}$, is first computed for an appropriately assumed optical model potential. If the optical-model potential had a spin–orbit interaction in it, one gets $C_{lj}^{(n)}$, instead of $C_l^{(n)}$, and thus the HF cros ssection is to be expressed in terms of $T_{lj}^{(n)}$, instead of $T_l^{(n)}$. In our calculation, the scattering coefficient is of the form $C_{lj,nl'j'}{}^J$ and thus our HF cross section is to be modified accordingly.

As is seen from (42) the scattering coefficient $C_{lj;nl'j'}$ is defined as the amplitude of the outgoing wave in the channel $(nl'j')$ when there is an incoming wave in the channel $(1lj)$ with the amplitude l exp $(i\sigma_l^{(1)})$, and can be used in defining the penetrabilities in the ground state channels as is seen below. Since we need the penetrabilities in the excited channels too, we shall extend the scattering coefficient $C_{lj;nl'j'}{}^J$ into $C_{nlj;n'l'j'}{}^J$, which gives the amplitude of the outgoing wave in the channel $(n'l'j')$ when there is an incoming wave in the channel (nlj) with the amplitude l exp $(i\sigma_l^{(n)})$.

Using this generalized scattering coefficient, we first define a generalized S-matrix element $S_{nlj;n'l'j'}{}^J$ as[24]

$$S_{nlj;n'l'j'}{}^J=\delta_{nn'}\,\delta_{ll'}\,\delta_{jj'}+2iC_{nlj;n'l'j'}{}^J, \quad (55)$$

and use it to define the generalized transmission coefficient $T_{nlj}{}^J$ as

$$T_{nlj}{}^J=1-\sum_{n'l'j'}[l'^2/l^2]S_{nlj;n'l'j'}{}^JS_{nlj;n'l'j'}{}^{J*}. \quad (56)$$

Using (56) and the idea of detailed balance,[25] the contribution from the compound process to the scattering cross section leaving the target in its nth state may be given as[26]

$$\sigma_n{}^{(c)}(\theta)=(\pi/k_1^2)\sum_{ii'm_sM_1}(a_{m_s}{}^{(i)})^2(b_{M_1}{}^{(i')})^2\sum_J[1/\sum_{nlj}T_{nlj}{}^J]\cdot\sum_{ljl'j'(m)}(2l+1)(ls0m_s\mid jm_s)^2(jI_1m_sM_1\mid JM)^2\cdot(l'sm_l'm_s'\mid j'm_j')^2(j'I_nm_j'M_n\mid JM)^2\cdot T_{1lj}T_{nl'j'}\mid Y_{l'm_l'}\mid^2, \quad (57)$$

which is now independent on ϕ. Note that T_{nlj} is a real quantity.

D. Expression of the Amplitudes $a_{m_s}{}^{(i)}$ and $b_{M_1}{}^{(i')}$

In order to complete the description of the cross sections it would be desirable to give an explicit account on how the amplitudes $a_{m_s}{}^{(i)}$ and $b_{M_1}{}^{(i')}$ are computed. We begin the explanation with that for $b_{M_1}{}^{(i')}$.

It often is possible to choose an axis, say z' axis, in space, such that if this is chosen as the axis of quantization of the nuclear spin states, the state of polarization of that nucleus is completely described by giving the occupational probabilities $P(N_1)$ of the magnetic substates N_1, which satisfy the normalization condition

$$\sum_{N_1=-I_1}^{I_1}P(N_1)=1. \quad (58)$$

[22] W. Hauser and H. Feshbach, Phys. Rev. **87**, 366 (1952).
[23] P. A. Moldauer, Phys. Rev. **123**, 754 (1961); **129**, 968 (1963).
[24] G. R. Satchler, Phys. Letters **7**, 55 (1963).
[25] J. M. Blatt and V. F. Weisskopf, *Theoretical Nuclear Physics* (John Wiley & Sons, Inc., New York, 1952).
[26] An expression very close to this has been given in Refs. 3 and 4.

Since the amplitudes, that result from the scattering due to nuclei occupying these different magnetic substates, do not interfere with each other, N_1 can be used to specify different ensembles. In other words one can identify the set (i') as the set (N_1). Thus in general the total number of different ensembles equals $2I_1+1$.

As is seen in the explicit forms of the wave functions and the cross sections given above, the direction of incidence of the projectile was taken as the z axis, and it was also used as the axes of quantization along which all the magnetic quantum numbers appearing there were defined. If the z axis were parallel to the z' axis defined above, we could identify the magnetic quantum number N_1 with M_1 that appears as the suffix of the amplitude $b_{M_1}{}^{(i')}$ and thus one can put

$$b_{M_1}{}^{(i')}=b_{M_1}{}^{(N_1)}=[P(N_1)]^{\frac{1}{2}}\,\delta_{M_1N_1}. \tag{59}$$

In general, however, z and z' axes are not parallel to each other. In such cases let us assume that the orientation of the former relative to that of the latter is described by the Euler angles $(\theta_1, \theta_2, \theta_3)$. Then we get

$$b_{M_1}{}^{(i')}=b_{M_1}{}^{(N_1)}=D_{N_1M_1}{}^{(I_1)}(\theta_1, \theta_2, \theta_3)[P(N_1)]^{\frac{1}{2}}, \tag{60}$$

as a natural extension of (59), where $D_{M_1N_1}{}^{(I_1)}$ is the rotation matrix.[18] Clearly (60) reduces to (59) if $\theta_1=\theta_2=\theta_3=0$.

Since all the cross sections considered above contain the amplitude $b_{M_1}{}^{(N_1)}$ bilinearly, the over-all phase of $b_{M_1}{}^{(N_1)}$ is immaterial. We therefore understand that $[P(N_1)]^{\frac{1}{2}}$ means the positive square root of $P(N_1)$.

When the target is unpolarized, we can take z' parallel to z. Since furthermore, in this case, the occupational probabilities must be the same for all the values of N_1, $P(N_1)$ is equal to $1/(2I_1+1)$. From (59) we thus get

$$b_{M_1}{}^{(N_1)}=\delta_{N_1M_1}\hat{I}_1^{-1}. \tag{61}$$

Sometimes the state of polarization of the target is more complicated than can be described by (60). For example, a single crystal of the metal holmium under a comparatively weak magnetic field[12,27] consists of several domains, nuclei belonging to each domain having different orientation of the axis of quantization as defined above of Eq. (58). It should be noted, however, that the nuclei belonging to different domains belong to different ensembles in the sense that the waves scattered by nuclei belonging to different domains do not interfere with each other. Therefore, we can use (60), by taking appropriate Euler angles (θ_i) separately for each domain, in order to compute various cross sections. The theoretical cross sections that are to be compared with experiments are obtained by adding the cross sections corresponding to each type of domain weighted by its relative population.

In this way the use of the amplitudes $b_{M_1}{}^{(i')}$ allows us to handle rather complicated targets fairly easily.

Derivation of the amplitudes $a_{m_s}{}^{(i)}$ is exactly the same as that of $b_{M_1}{}^{(i')}$. It is enough simply to replace I_1 by s. Thus one gets, for example, for an unpolarized beam of $s=\frac{1}{2}$ projectile,

$$a_{\frac{1}{2}}{}^{(1)}=a_{-\frac{1}{2}}{}^{(2)}=(\tfrac{1}{2})^{\frac{1}{2}} \quad \text{and} \quad a_{-\frac{1}{2}}{}^{(1)}=a_{\frac{1}{2}}{}^{(2)}=0; \tag{62}$$

while for a beam polarized in the x direction by $P\%$, a situation often met with in the actual experiments, one has

$$\begin{aligned} a_{\frac{1}{2}}{}^{(1)}&=a_{-\frac{1}{2}}{}^{(1)}=\tfrac{1}{2}(1+P/100)^{\frac{1}{2}},\\ a_{\frac{1}{2}}{}^{(2)}&=-a_{-\frac{1}{2}}{}^{(2)}=\tfrac{1}{2}(1-P/100)^{\frac{1}{2}}. \end{aligned} \tag{63}$$

V. ADIABATIC APPROXIMATION

We can make use of the adiabatic approximation[14,15] in the coupled-channel calculation when the following three requirements are satisfied: (a) The target nucleus is well deformed and thus its excitation spectrum is closely that of an ideal rotational band; (b) the incident energy of the projectile is much higher than the excitation energies of the above rotational states; (c) we are interested in the excitation only of the states which belong to the ground-state rotational band.

When this approximation is used, the coupling to *all* states of the ground band is included automatically, and therefore (when the above requirements are satisfied) one can get quite accurate theoretical results with less complicated and thus much faster machine calculations, than when the nonadiabatic coupled-channel calculation is made.

Recently Barrett[15] gave a formulation of the adiabatic coupled-channel calculation (abbreviated in the following as ACC, compared with the nonadiabatic coupled-channel calculation which is abbreviated as NACC) in a form particularly suited for the coding of a computer program. His formulation, however, included neither Coulomb nor spin–orbit interaction, and thus could be used only when the scattering of neutrons is considered under the assumption that the spin–orbit interaction is negligibly small, which does not seem to be the case in general. For more practical purposes, it is therefore necessary to extend Barrett's formulation.

The potential we start with is the same as that given in (1), and since we assume again that the target nucleus and thus the potential which it exerts on the projectile is axially symmetric, the radii R and $\bar{R}$ are given by (3). If (3) is inserted into (1), and the latter is expanded in terms of the Legendre polynomials, one gets (14) again. Since we prefer, however, because of reasons which we shall see shortly, to write down the coupled equations referring to the body-fixed coordinate system, we write $V_{\text{coupl}}{}^{(r)}$, instead of (15), as

$$V_{\text{coupl}}{}^{(r)}=\sum_{\lambda(\lambda\neq 0)} v_{cp}{}^{(\lambda)(r)}(r)\,Y_{\lambda 0}', \tag{64}$$

where $v_{cp}{}^{(\lambda)(r)}(r)$ is the same as in (16). The prime attached to $Y_{\lambda 0}'$ in (64) means that its arguments are polar angles referred to the body-fixed system.

Denoting by $\bar{m}_j$ the projection along the nuclear

[27] Cf. Sec. VII B2.

symmetry axis of the total angular momentum j of a partial wave of the projectile, the total wave function in the internal region may be written as

$$\Psi = r^{-1}\sum_{lj\bar{m}_j} R_{lj\bar{m}_j}(r)\,\mathcal{Y}'_{lj\bar{m}_j}. \tag{65}$$

Using (14), (64), and (65) the coupled equation is easily written down as

$$\left(\frac{d^2}{d\rho^2}-\frac{l(l+1)}{\rho^2}-E^{-1}V_{\text{diag}}+1\right)R_{lj\bar{m}_j} = E^{-1}\sum_{l'j'}\langle \mathcal{Y}'_{lj\bar{m}_j} \mid \sum_{\lambda} v_{cp}{}^{(r)(\lambda)}(r)\,Y'_{\lambda 0} \mid \mathcal{Y}'_{l'j'\bar{m}_j}\rangle R_{l'j'\bar{m}_j}. \tag{66}$$

The similarity and difference between (23) and (25) on the one hand, and (65) and (66) on the other hand are worth noting. One can easily derive (65) and (66), respectively, from (23) and (25) by deleting all the quantities which describe the properties of the target, by replacing J by $\bar{m}_j$, and then quantizing the angular momenta with respect to the body-fixed system rather than the space-fixed system.

The reason why the body-fixed system was preferred is clear from (66), because otherwise there would be coupling between partial waves with different values of $\bar{m}_j$, in addition to the coupling between those with different values of j.

The evaluation of the coupling matrix that appear in the right-hand side of (66) is straightforward and one gets

$$\langle \mathcal{Y}'_{lj\bar{m}_j} \mid \sum_{\lambda} v_{cp}{}^{(r)(\lambda)} Y_{\lambda' 0} \mid \mathcal{Y}'_{l'j'\bar{m}_j}\rangle = \sum_{\lambda} v_{cp}{}^{(r)(\lambda)}(r)\left[(4\pi)^{-\frac{1}{2}} \hat{l}\hat{l}'\hat{j}\hat{j}'\hat{\lambda}^{-1}(-)^{\frac{1}{2}(l'-l)}(ll'00 \mid \lambda 0)\cdot W(ll'jj';\lambda s)\,(-)^{s+\bar{m}_j}(jj'-\bar{m}_j\bar{m}_j \mid \lambda 0)\right]. \tag{67}$$

Comparing this expression with those that appeared in Sec. IV, we see that the matrix which was called the B matrix there is now replaced by a c number, which is unity, and the whole coupling matrix is completely geometrical [except for the radial functions $v_{cp}{}^{(r)(\lambda)}(r)$].

Corresponding to the derivation of (65) and (66) from (23) and (25), the asymptotic form of the total wave function may be derived from (42) as

$$\Psi_{\text{asym}} = \left[(4\pi)^{\frac{1}{2}}/rk_1(v_1)^{\frac{1}{2}}\right]\sum_{(ii')m_s M_1} a_{m_s}{}^{(i)} b_{M_1}{}^{(i')} \cdot \sum_{lj}(ls0m_s \mid jm_s) D_{m_s\bar{m}_j}{}^{i}(\theta_i)\sum_{l'j'}\hat{l}'\exp(i\sigma_{l'}{}^{(1)}) \cdot\left[\delta_{ll'}\,\delta_{jj'}F_{l'}{}^{(1)} + C_{lj;l'j'}{}^{\bar{m}_j}(G_{l'}{}^{(1)}+iF_{l'}{}^{(1)})\right] \cdot \mathcal{Y}'_{l'j'\bar{m}_j}\Phi_{I_1M_1}. \tag{68}$$

Contrary to (65) and (66) there appear factors in (68) which describe properties of the target nucleus. There exists, however, an important difference, between (68) and (42), in that in the former no coupling of the angular momenta I_1 and j occurs. This is a consequence of the adiabatic approximation which supposes that the target nucleus is inert during the scattering process, and thus carries no angular momentum dynamically. The reason why we had a rotation function $D_{m_s\bar{m}_i}{}^{i}(\theta_i)$, whose arguments θ_i describe the Euler angles between the body- and space-fixed coordinates, is that (68) was first obtained in the space-fixed system and then transformed into the body-fixed system. With the form of (68) the construction of matching equation to (65) is clearly understood.

Using the same technique as was used in deriving the scattered wave (46) from (42), we now derive the scattered wave $\Psi_{\text{scatt}}{}^{(\text{ACC})}$ from (68) as

$$\Psi_{\text{scatt}}{}^{(\text{ACC})} = \frac{\exp(i\rho_1 - i\eta_1 \ln(2\rho_1))}{r(v_1)^{\frac{1}{2}}}\sum_{(ii')m_sM_1} a_{m_s}{}^{(i)} b_{M_1}{}^{(i')} \cdot\left[f_c(\theta)\chi_{sm_s} + \left[(4\pi)^{\frac{1}{2}}/k_1\right]\sum_{ljl'j'\bar{m}_j m_s' m_l' m_j'}\hat{l}'\exp(2i\sigma_{l'}{}^{(1)}) \cdot C_{lj;l'j'}{}^{\bar{m}_j}(ls0m_s \mid jm_s)(l'sm_l'm_s' \mid j'm_j') \cdot D_{m_s\bar{m}_i}{}^{i}\, D_{mj'\bar{m}_i}{}^{*j'} Y_{l'm_l'}\chi_{sm_s'}\right]\Phi_{I_1M_1}. \tag{69}$$

A new rotation function $D_{m_i'\bar{m}_j}{}^{j'*}$ appears in (69), since the surface harmonics $Y_{l'm_l'}$ is expressed in terms of the polar angles referred to the space-fixed system.

If the right-hand side of (69), excepting the factor $\exp(i\rho_1 - i\eta_1 \ln(2\rho_1))/(r(v_1)^{\frac{1}{2}})$, is expanded in terms of the eigenfunctions $\Phi_{I_nM_n}$ of the target states, each expansion coefficient gives just the scattering amplitude that leave the target in that particular state. The evaluation of this expansion coefficient is easily made, if one notes that $\Phi_{I_nM_n}$ is written as

$$\Phi_{I_nM_n} = \left[(2I_n+1)/8\pi^2\right]^{\frac{1}{2}} D_{M_nK}{}^{I_n}(\theta_i), \tag{70}$$

where K is the projection of I_n to the nuclear symmetry axis.

Instead of giving this expansion coefficient, however, we give a closely related amplitude $X_{m_sM_1,m_s'M_1'}{}^{(\text{ACC})}(\theta,\phi)$, which plays exactly the same role as the amplitude $X_{m_sM_1,m_s'M_1'}(\theta,\phi)$ given in (48) did;

$$X_{m_sM_1;m_s'M_n}{}^{(\text{ACC})}(\theta,\phi) = f_c(\theta)\;\delta_{n1}\,\delta_{m_sm_s'}\,\delta_{M_nM_1} + \sum_{ljl'j'\bar{m}_j m_l' m_j'}\left[(4\pi)^{\frac{1}{2}}/k_1\right]l'\exp(2i\sigma_{l'}{}^{(1)})\,C_{lj;l'j'}{}^{\bar{m}_j} \cdot (ls0m_s \mid jm_s)\sum_{JM_J}\left[(-)^{\bar{m}_j-m_j'}\hat{I}_1\hat{I}_n{}^{-1}(I_1JK0 \mid I_nK)\right. \cdot (I_1JM_1M_J \mid I_nM_n)(jj'\bar{m}_j - \bar{m}_j \mid J0) \left.(jj'm_s - m_j' \mid JM_J)(l'sm_l'm_s' \mid j'm_j')\,Y_{l'm_l'}(\theta,\phi)\right]. \tag{71}$$

Similarity between (71) and (48) is again remarkable. Expressions for various cross sections and polarizations derived for NACC in Sec. IV can be used for ACC by simply replacing the amplitudes $X_{m_sM_1,m_s'M_1'}(\theta,\phi)$ and $Z_{m_sM_1,m_s'M_1';l'}$, respectively, by $X_{m_sM_1,m_s'M_n}{}^{(\text{ACC})}(\theta,\phi)$

and by

$$Z_{m_s M_1, m_s' M_1'; l'}^{(\mathrm{ACC})} = \sum_{jlj'\bar{m}_j m_l l' m_j'} (lsom_s \mid jm_s) C_{lj;l'j'}^{\bar{m}_j} \cdot (l'sm_l'm_s' \mid jm_j') \sum_{JM} [(-)^{\bar{m}_j - m_j'} (I_1 JK0 \mid I_1 K) \cdot (I_1 JM_1 M_J \mid I_1 M_1') (jj'\bar{m}_j - \bar{m}_j \mid J0) \cdot (jj' m_s - m_j' \mid JM_J)]. \quad (72)$$

We close this section with several remarks which are important from the practical point of view of the numerical calculations.

As is easily seen from (67), the coupling matrix element is multiplied by a phase factor $(-)^{j+j'+\lambda+2s}$ if $\bar{m}_j$ is changed into $-\bar{m}_j$. Therefore, [when the parity of λ is unique, as is the case for a pure quadrupole deformation of the target where we have $(-)^{\lambda}=1$], there holds a relation

$$C_{lj;l'j'}^{-\bar{m}_j} = (-)^{j+j'+2s} C_{lj;l'j'}^{\bar{m}_j}. \quad (73)$$

On the other hand, the factor in the square bracket in (71) and (72) is multiplied by $(-)^{j+j'+J+2s}$ if $\bar{m}_j$ is changed into $-\bar{m}_j$. Thus the summation over $\bar{m}_j$ in (71) and (72) can be limited, say to nonnegative values $\bar{m}_j$ if the bracket factor is multiplied by $(1+(-)^J)/(1+\delta_{\bar{m}_j,0})$ at the same time. In other words the coupled equation (66) is needed to be solved only for nonnegative $\bar{m}_j$, which means a large saving in the machine time and the core storage needed for the computation.

Based on this fact and the form of (66), let us now consider how much numerical work is involved in solving the coupled equations. We first assume that we have found somehow a quantity $j_{\max}$, which is the maximum value of j of the partial waves that give nonnegligible contribution to the scattering. We also assume, for definiteness, that the spin of the projectile is $s=\frac{1}{2}$. Then when $\bar{m}_j=\frac{1}{2}$, (67) is a coupled equation between partial waves whose j ranges from $\frac{1}{2}$ to $j_{\max}$, and thus is a coupled equation between $n_c=j^{\max}+\frac{1}{2}(\equiv n_c^{\max})$ functions. When $\bar{m}_j=\frac{3}{2}$, $j=\frac{1}{2}$ wave is not coupled together and thus n_c reduces to $n_c^{\max}-1$. In this way each time $\bar{m}_j$ is increased by unity, n_c is decreased by unity and finally when $\bar{m}_j=j_{\max}$ we have a single uncoupled equation.

Thus, what the computer has to do for each given value of the parity operator $\Pi=(-)^l=\pm 1$ is to solve a n_c-coupled equation only once for each value of n_c ranging from $j_{\max}+\frac{1}{2}$ to unity. Therefore unless $j_{\max}$ is extremely high (i.e., unless the incident energy is extremely high) the machine time needed in solving the coupled equation in ACC is much shorter compared with that made with NAAC where N_c coupled equation [cf. Eq. (20)] had to be solved many ($\approx J_{\max}$) times. Another, and perhaps more important merit concerning the machine time of ACC over NACC is that the sizes of the coupled equations to be solved are unchanged, if the incident energy is fixed, irrespective of how high we go up in the excited states to calculate the scattering cross sections.

When the spin s of the projectile is zero, $j_{\max}$ defined above becomes an integer $l_{\max}$, say, and $n_c^{\max}$ is reduced to

$$n_c^{\max}=l_{\max}/2; \quad (l_{\max}=\text{even}),$$
$$n_c^{\max}=(l_{\max}+1)/2; \quad (l_{\max}=\text{odd}), \quad (74)$$

which is only half of its value for $s=\frac{1}{2}$. Therefore in this case the computation can be made very quickly.

VI. REMARKS ON THE NUMERICAL CALCULATIONS

Based on the formulation developed in Secs. II through V, a program was written to be run on the CDC-1604 computer at Oak Ridge. The detailed account of the coding of this program is to be published elsewhere. This program was written in such a general and flexible way, that only a single binary program is needed in order to perform all the calculations that are presented in this and the next sections, and also other calculations to be reported in the future.

Our theoretical results show very good agreement with experiment in most of the cases considered. In the course of trying to obtain such agreement, a number of interesting features were found concerning the dependence of various cross sections on the parameters and the assumed scheme of the coupling. (We mean by "scheme of coupling" the set of states of the target nucleus between which the strong coupling is considered and the type of such coupling.) In the present section we give a brief account of such general features; knowledge of which will make easier future attempts to fit the theory to experiments in a way similar to the examples given in the next section.

The radial factors of the coupling terms given in (13.1), (13.2), and (16) are complex in general. In the literature[3,7] the imaginary terms were usually neglected. If this is done, we say that our calculation is made with RFF, meaning that we use real form factors, while if the whole complex factors are used we say that the calculation is made with CFF (complex form factor). As was defined in Sec. V, ACC and NACC mean, respectively, the adiabatic and nonadiabatic calculations.

It is also convenient to give a standard set of optical model parameters. In most of the calculations the projectiles considered are nucleons, and for nucleons the following set of parameters given by Perey[16] is found to be usually very good, if the energy of the nucleons is not too large; less than, say, 30 MeV. Therefore we used this set as much as possible:

$$r_0=\bar{r}_0=r_c=1.25 \text{ F}, \quad a=0.65 \text{ F},$$
$$\bar{a}=0.47 \text{ F } (A<150), \quad a=0.76 \text{ F } (A>150),$$
$$V_{s0}=7.5 \text{ MeV}, \quad W=0.0 \text{ MeV}. \quad (75)$$

The set of radius parameters r_0, $\bar{r}_0$, and r_c and the diffuseness parameters a and $\bar{a}$ is sometimes called the "geometrical parameters."

Contrary to the fixed parameters of (75), the parameters V and W_D are varied from case to case in order to get a good agreement of the theory to experiment, but the following are a standard set of values of these parameters which provide a good starting point;

$$V=(52.2-0.3E)\text{ MeV}, \qquad W_D=11.5\text{ MeV}. \quad (76)$$

This V is for protons. For neutrons it is larger than (76) by a few MeV. W_D of (76) is good when no coupling is considered. It is a rather sensitive function of the coupling scheme.

We also give here an idea of how the machine time T needed in performing a particular calculation varies depending on the coupling scheme and the parameters involved in each calculation. Most of the machine time is taken in solving numerically the coupled equations (25) in NACC or (66) in ACC. The time needed in solving a n_c-coupled equations is roughly proportional to n_c^3 times R_m, where R_m is the matching radius. If NACC is used, N_c-coupled equations have to be solved $J_{\max}(=I_1+j_{\max})$ times as was mentioned below Eq. (20), where N_c, I_1, and $j_{\max}$ were defined in the beginning of Sec. III. This $J_{\max}$ is roughly proportional to k_1R_0 and thus T is proportional to $N_c^3R_mk_1R_0$. Since further R_m and R_0 are both proportional to $r_0A^{\frac{1}{3}}$, we can write

$$T=cr_0^2A^{\frac{1}{3}}k_1N_c^3. \quad (77)$$

Here c is a constant and is very roughly of the order of 0.01 sec when our code is run on the CDC 1604. (r_0 and k_1 are measured in F and F^{-1}, respectively.) This figure is when RFF is used. If CFF is used, c has to be doubled. If higher-order terms that were neglected in (5) are considered, c increases roughly in proportion to the total number of terms in the coupling potential. When ACC can be used, T is reduced very much as was emphasized in Sec. V.

(i) We first consider how the cross sections vary when a particle is scattered, on the one hand, by a deformed nucleus, and on the other hand, by a vibrational nucleus, but of the same A (mass number) and Z (atomic number). Such calculations were suggested to the author by Bohr.[28] The result shown in Fig. 1 is an example which was made with $A=156$ and $Z=64$ for a 17.5-MeV proton. Since these A and Z are those for ^{156}Gd, and since ^{156}Gd is a well-deformed nucleus, the deformed nucleus calculation is realistic, while the vibrational calculation is hypothetical. Nevertheless, since the theoretical cross sections are rather insensitive to a slight change of A, we can expect that the results given here predict the general features of what one would observe if he bombards, with protons of the above energy, several isotopes, of, say, Sm or Nd, whose lightest and heaviest stable elements are, respectively, vibrational and deformed nuclei.

[28] A. Bohr (private communication).

The solid lines [which are the same both in Figs. 1(A) and 1(B)] were calculated under the deformed nucleus assumption by using CFF and ACC. (These curves are realistic and, as is seen in Sec. VII-B are in good agreement with experiment.) The optical-model parameters used are (75), $V=50$ MeV, and $W_D=7.5$ MeV. In the potential (16) the summation over λ' is restricted to a term with $\lambda'=2$, and β_2 is put equal to 0.32.

The dotted lines in Fig. 1 are calculated by assuming an ideal 0^+–2^+–4^+ vibrational level scheme. The calculation was made with CFF, using the same optical-model parameters as in the deformed case. The elements of the coupling matrices to be used are found in (36.1), (36.2), and (37.1), and in all these elements a common single value of β_2 is used; (hence we assume an *ideal* vibrational nucleus). The value of β_2 used was 0.32 in Fig. 1(A), in accord with the deformed nucleus calculation, while it was 0.20 in Fig. 1(B), a value of the order of magnitude that is found in many actual vibrational nuclei. A remarkable feature observed in Fig. 1 is that the structure of the cross-section curve is much more pronounced in the vibrational case than in the deformed case.

Comparison between the vibrational curves in Figs. 1(A) and 1(B) shows that the structure is rather insensitive to β_2, but the magnitudes of the cross sections varies. If β_2 is sufficiently low the cross section to the 2^+ state is expected[7] to be proportional to β_2^2 and that to the 4^+ state to β_2^4. Since our β_2 is large, the saturation

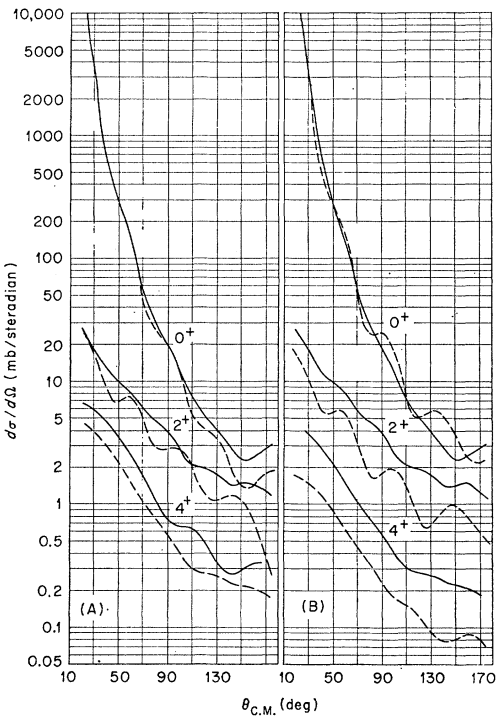

FIG. 1. Scattering cross sections of 17.5-MeV protons by a nucleus with $A=156$ and $Z=64$. Solid lines are for deformed nucleus and dotted lines are for vibrational nucleus.

phenomenon[7] has already occurred and the 2^+ cross section is reduced by going from Fig. 1(A) to Fig. 1(B) by a factor 1.5 which is about half the ratio of the two values of β_2^2, i.e., 2.6. The reduction factor of 4^+ cross section is 3.3, which is again about half of the ratios of the two values of β_2^4, i.e., 6.5.

(ii) Next we shall see how the elastic scattering cross section varies depending on whether the coupling to the higher states is considered or not. We reproduce in Fig. 2 the elastic cross section curve of Fig. 1. In Fig. 2(A) the curve 1 is the same as the dotted elastic cross section curve of Fig. 1(B), while that in Fig. 2(B) is for the deformed case of Fig. 1. As mentioned in (i), W_D was taken as 7.5 MeV in obtaining these curves.

The two curves 2 and 3 of Fig. 2(A) are the results of uncoupled calculations for the elastic scattering with $W_D=7.5$ MeV and 11.5 MeV, respectively. As is seen, the curves 2 and 3 brackets the curve 1 in most of the angular range, and this suggests that by taking W_D which is in between the above two values, one can get a curve that coincides with the curve 1. In fact we found that the result with $W_D=9.5$ MeV coincides with the latter almost perfectly. This result is quite important since it indicates that about 20% of the absorptive potential observed in the (pure) elastic channel is accounted for by the coupling to the 2^+ state (when $\beta_2=0.2$).

In the actual calculations which aim to fit the experimental data on the scattering cross sections from vibrational nuclei, we found the following procedure

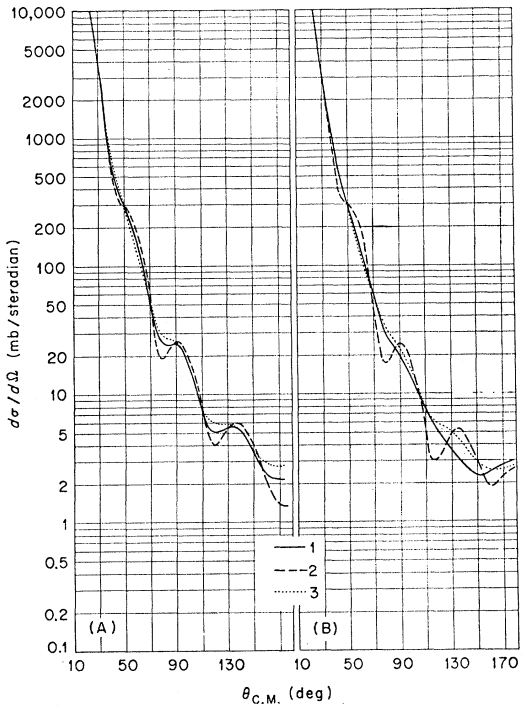

FIG. 2. Dependence of the elastic scattering cross section on the coupling schemes and the parameter W_D. (A) vibrational nucleus; (B) rotational nucleus.

is very powerful and time saving. First of all, we discovered that the geometrical parameters of (75) were usually very good. Therefore we keep them fixed. By taking the differential cross-section data of the elastic scattering, we first adjust V, W_D, and sometimes V_{SO}, to fit the experiment. This calculation can be made very quickly (a few seconds per run); cf. Eq. (77). We then consider the experimental cross section to the first excited 2^+ state and perform the 0^+–2^+ coupling calculation by reducing the value of W_D obtained in the pure elastic calculation by about 20%, and then adjust β_2 to fit the data. (This step is still fairly fast; one or two minutes per run). In this case the fit to the elastic cross section is usually guaranteed, as we have seen in Fig. 2(A). We then couple, if there exist data, to the two-phonon states. Since this coupling reduces the cross section to the first excited 2^+ state, we increase the previously obtained β_2 value by about 10%, still guaranteeing the fit both of the elastic and first 2^+ state cross sections. The β_2 values to be used for the coupling between the one- and two-phonon states are then adjusted to fit the cross section curve of each two-phonon 0^+, 2^+, and 4^+ states. These β values are usually found to be smaller than that used between the ground and the first 2^+ states, and the square of the former divided by the latter gives the factors by which the $B(E2)$ values between the two- and one-phonon states are reduced. In turn, this is a measure of how badly the simple harmonic nature of the vibrations is violated in the nucleus under investigation. Thus it is a very important quantity from the nuclear structure point of view. Until recently these reduction factors were supplied almost exclusively from Coulomb excitation experiments. As was found by Buck[6,29] and as is seen in the next section, inelastic scattering data and its analysis in terms of the coupled-channel calculation is beginning to be a very powerful tool for such purposes.

(iii) The situation concerning the elastic cross section for a deformed nucleus is not so simple as for a vibrational nucleus. Since we use a Legendre polynomial expansion, as emphasized in Sec. II(ii), the diagonal part of the optical model potential (14) is not the same as that of (12) if $\beta_2\neq 0$. Therefore even if we cut off the coupling to the higher state (we now consider NACC instead of ACC of Fig. 1), the elastic-scattering cross section is still a function of β_2. The curves 2 and 3 of Fig. 2(B) are the results of the uncoupled elastic scattering calculation with $\beta_2=0.32$ and $W_D=7.5$ and 15.0 MeV, respectively. In about half the angular range these two curves lie on a same side of the curve 1, so in this case the simple adjustment of W_D cannot reproduce the result of the coupled-channel calculation. In other words we cannot follow such a procedure as to increase the number of coupled states step-by-step as we did in the case of vibrational nuclei. If we use ACC, however, this fact does not matter, since we have to solve the full size coupled equations all the

[29] H. W. Broek, J. L. Yntema, B. Buck, and G. R. Satchler, Nucl. Phys. (to be published).

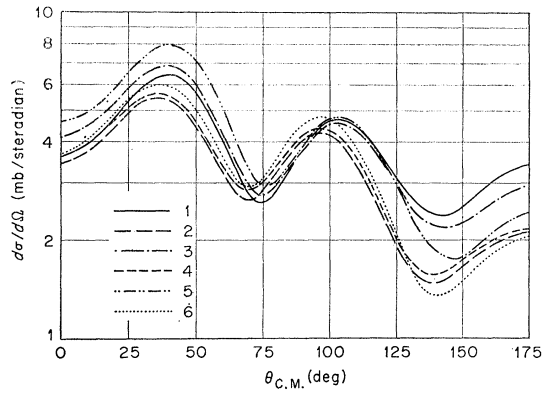

FIG. 3. Differential cross section of 12.16-MeV protons to the octupole 3^- state in ^{114}Cd under various coupling schemes.

time, irrespective of how many excited states we consider.

(iv) Corresponding to the discussion in (ii) concerning the dependence of the elastic-scattering cross section on the parameter W_D and the coupling scheme, it is interesting to see how they affect the cross section of the one-phonon state. We take ^{114}Cd and first consider the following coupling scheme: 0^+ (ground state) -2^+ (one quadrupole-phonon state at 0.56 MeV) -3^- (one octupole-phonon state at 1.95 MeV) -3^- (one-quadrupole–one-octupole phonon state at 2.51 MeV, c.f. Sec. VII A2).

The differential cross section to the 3^- state at 1.95 MeV, calculated for 12.16-MeV protons with the above coupling scheme and with CFF and then with RFF are shown, respectively, as curves 1 and 2 in Fig. 3. The optical model parameters used were (75), $V=48.8$ MeV and $W_D=12.2$ MeV. The coupling matrices are constructed by using (36.1), (36.4), (36.5), (37.3), and (37.4) with $\beta_2=0.2$ and $\beta_3=0.136$. As is seen in Fig. 9 below, the curve 1 has a shape that fit the experiment in that the first and the second peaks appear at $\theta=43°$ and $\theta=105°$, and that the first valley appear at $\theta=75°$. The corresponding peaks in curve 2 appear at $\theta=35°$ and 95° and the valley appears at $\theta=70°$ and thus this curve fits the experiment less well than curve 1, indicating that the CFF is preferred in this case.

We next consider the 0^+–2^+–3^- coupling scheme, cutting off the coupling to the second 3^- state in the above calculation. The resulting 3^- cross section is given as curves 3 and 4 in Fig. 3 for CFF and RFF, respectively. It is seen that their shapes are similar to the corresponding curves 1 and 2, but the magnitudes are slightly increased. A similar feature has already been noticed in (ii) in comparing the one-phonon 2^+ state cross sections which were obtained with and without the coupling to the two-phonon states.

The curves 5 and 6 of Fig. 3 were obtained, again with CFF and RFF, respectively, but assuming only the 0^+–3^- coupling, and it is seen that their magnitudes (particularly at forward angles) are further increased compared to their corresponding curves 3 and 4. This result may seem surprising considering the fact that in the above 0^+–2^+–3^- calculation the 2^+ and 3^- states were coupled together only indirectly through separate coupling to the ground state. We should recall, however, that with $\beta_2=0.2$ about 20% of the absorption in the ground channel was accounted for by the 0^+–2^+ coupling. Since this coupling was cut-off in the 0^+–3^- calculation, we should have used a value of W_D in the ground state channel which was 20% larger than that used in the 0^+–2^+–3^- calculation in order to obtain the same elastic scattering. The actual calculation showed, however, that the increment of W_D by 20% was too large, but if the increment was 10% the 0^+–3^- calculation gave a 3^- cross section which agreed very well with that obtained in the 0^+–2^+–3^- calculation. [A similar comparison, as made in (ii), of the elastic cross sections with and without the 0^+–3^- coupling was made which showed that about 10% of the absorptive potential in the ground channel was accounted for by the 0^+–3^- coupling if β_3 was of the order of 0.14.]

As another example of the dependence of the excitation cross sections on the coupling scheme, it would be interesting to see with what accuracy we can approximate a 0_0^+–2_1^+–0_2^+–2_2^+–4_2^+ (the suffix means the phonon number in each state) coupling calculation by performing separately the 0_0–2_1–0_2, 0_0–2_1–4_2 coupling calculations. For that purpose we compared the results of the 0_0^+–2_1^+–2_2^+ and 0_0^+–2_1^+–0_2^+–2_2^+–4_2^+ coupling calculations for the scattering of 17.5-MeV protons by ^{64}Zn, assuming $\beta_2=0.2$ in all the matrix elements. The results showed that, for example, the 2_2^+ cross sections in the former case was about 10% larger than that of the latter case (though the shape was the same) which indicates that the above-mentioned separate calculations can cause as much as 5% error in the β values.

As emphasized in (ii), the purpose of performing the coupled-channel calculation and fitting the experiment is to find out what β_λ values we should use between various collective states. The preceding arguments show, however, that the theoretical cross sections change their magnitudes depending on what coupling scheme was used for a given value of β_λ. In other words the β_λ values deduced by fitting the experiment depend on the coupling scheme used in each calculation. This ambiguity could be removed, of course, if a sufficiently large number of excited states were coupled together (and if it is assumed that the same W_D can be used in all the channels). Unfortunately, however, such a calculation with a very large number of coupled states cannot be performed with the presently available computers. In some of the calculations which are given in the next section the effect of the neglected coupling to the possible higher excited states are taken into account phenomenologically by using larger values of

W_D in the higher excited coupled states than that are used in the lower coupled states (Cf., e.g., Sec. VII A2).

The analysis of Coulomb excitation is a variety of coupled-channel calculations (at least when the excitation probability is large as when collective states are excited by heavy ions), although the technique usually used[30] in solving the coupled equation appearing there is quite different from that used in the present paper. Therefore, although in the Coulomb excitation there exists nothing that corresponds to W_D, and thus the situation is less ambiguous, the dependence of the deduced β_λ [or $B(E\lambda)$] on the assumed coupling scheme still remains. In obtaining the $B(E2)$ values between the one- and two-quadrupole-phonon states in vibrational nuclei, it was so far customary[31] to use the formulas[32] which is based on the perturbation theory. These formulas certainly neglected the coupling of the two-phonon states to the three-phonon states. Although theories were developed[30] to avoid the perturbation (in the coupling terms) and couple many states at a time, their applicability is again restricted by the smallness of the suddenness parameter ξ. In order to get more accurate results for the β_λ values to be deduced, clearly some refinement is to be made for the Coulomb excitation calculation, as well as for our coupled-channel calculations. *Note added in proof.* We learned recently that a new technique has been developed by J. de Boer and A. Winther to treat the Coulomb excitation process with a high accuracy (J. de Boer, private communication).

(v) The dependence of various cross sections on the coupling scheme is more clearly seen if one compares the result of the NACC calculations for deformed nuclei with those of the ACC calculations, and such comparison is made here. In Fig. 4(A) we show results of calculations made for the scattering of 17.5-MeV protons by ^{165}Ho whose lowest states are members of a $K=7/2^-$ rotational band. The solid lines are the result of a NACC calculation with RFF and with the $7/2^-$–$9/2^-$–$11/2^-$ coupling, by using the optical model parameters of (75), $V=50.0$ MeV and $W_D=7.5$ MeV, and $\beta_2=0.30$. The dotted curves are the corresponding results of an ACC calculation with the same parameters.

As emphasized in Sec. V, the ACC calculation automatically takes into account the coupling of all the members of the ground state rotational band. Since the low excitation energies of the states of ^{165}Ho and the high energy of the incident proton guarantee the validity of the ACC calculation, the ACC results are more accurate in this case than those of the NACC.

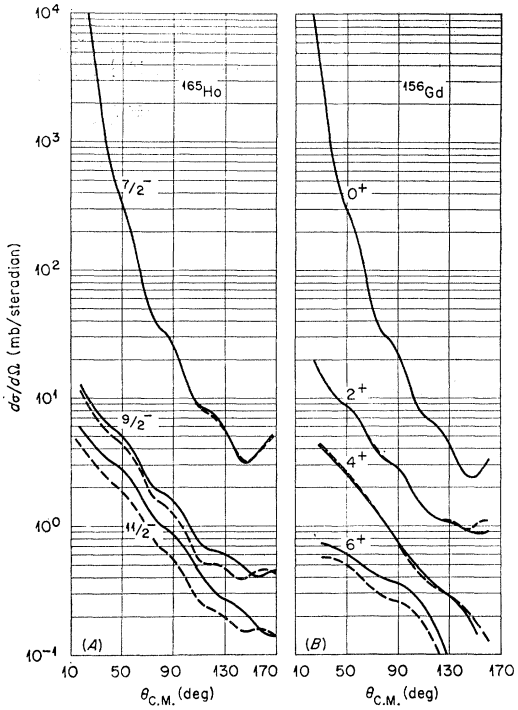

FIG. 4. Comparison of ACC (dotted lines) and NACC (solid lines) calculations for the scattering of 17.5-MeV protons by ^{165}Ho and ^{156}Gd.

A feature that is clearly seen in Fig. 4(A) is that the two curves for the $7/2^-$ state almost agree with each other, while for the other two states NACC gives a larger cross section than ACC does. This result is quite natural since in the NACC calculation the strong quadrupole coupling of the $9/2^-$ state to the $13/2^-$ state and that of the $11/2^-$ state to the $13/2^-$ and $15/2^-$ states were artificially cut-off, while all the possible strong quadrupole couplings of the ground $7/2^-$ state to the higher states were taken into account. If in NACC the coupling to the $13/2^-$ and $15/2^-$ states were also considered, the cross sections to the $9/2^-$ and $11/2^-$ states would have been reduced so as to agree with that of the ACC, but such calculation is too extensive to be made with the presently available computer. Even with the $7/2^-$–$9/2^-$–$11/2^-$ coupling, the number N_c of (20) is already thirty and the machine time needed for one run was about seven hours.

The curves in Fig. 4(B) are the results of corresponding calculations performed for the scattering of 17.5-MeV protons by ^{156}Gd. The optical-model parameters used were the same as in Fig. 4(A), but β_2 was 0.33. The relation between the NACC and ACC results is qualitatively the same as in Fig. 4(A). Namely, in the NACC calculation in which 0^+–2^+–4^+–6^+ coupling was considered, all the strong quadrupole coupling of the 0^+, 2^+, and 4^+ states to the higher excited states were taken into account, but the coupling of the 6^+ state to the 8^+ state was not. Therefore the NACC

[30] K. Alder and A. Winther, Kgl. Danske Videnskab. Selskab, Mat. Fys. Medd. **32**, No. 8 (1960); D. W. Robinson, Nucl. Phys. **25**, 459 (1961).

[31] See, e.g., F. K. McGowan, R. L. Robinson, P. H. Stelson, J. L. C. Ford, and W. T. Milner, Bull. Am. Phys. Soc. **9**, 107 (1964) and work to be published; D. Eccleshall, B. M. Hind, M. T. L. Yates, and N. McDonald, Nucl. Phys. **37**, 377 (1962).

[32] K. Alder, A. Bohr, T. Huus, B. Mottelson, and A. Winther, Rev. Mod. Phys. **28**, 432 (1956); A. C. Douglas, Nucl. Phys. **42**, 428 (1963).

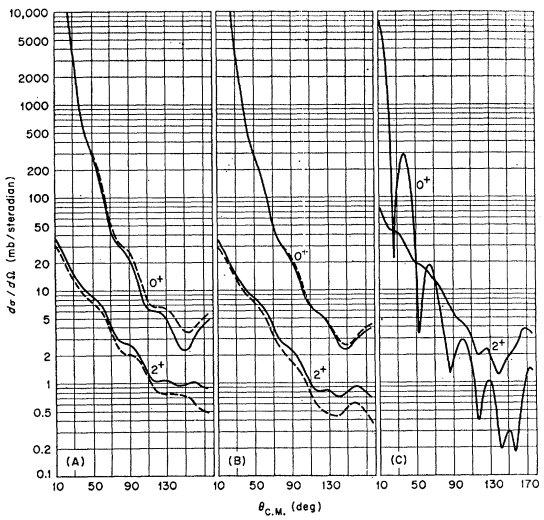

FIG. 5. (A) and (B): Comparison of the scattering of 17.5-MeV protons by ^{156}Gd made by using power series (dotted lines) and Legendre polynomial (solid lines) expansions of the interaction potentials. (C) Scattering of 17.5-MeV neutrons by ^{156}Gd.

and ACC results agreed with each other for the lower three states, but the NACC cross section to the 6^+ state was too large compared to the corresponding ACC cross section. Thus the results shown in Fig. 4 are quite reasonable.

(vi). In Sec. II [above Eq. (15)], we remarked that for deformed nuclei with large β_2, the expansion of potential (1) and (3) in powers of β_2 is a rather poor approximation and thus we should use a Legendre polynomial expansion. In order to see how bad the power series expansion is, we show several curves in Figs. 5(A) and 5(B), which were calculated for ^{156}Gd with the same parameters as used in Fig. 4(B).

All the curves in Figs. 5(A) and 5(B) are the results of ACC calculations. There the dotted and solid curves were obtained by using coupling terms that were derived by the power series and the Legendre polynomial expansions, respectively. For Fig. 5(A) only the first term of (13) (with $\lambda=2$) or the term in (15) with $\lambda=2$ was considered, while for Fig. 5(B) the second term of (13) or the $\lambda=4$ term of (15) was also included.

The results of the power series expansion are drastically different from those of the Legendre polynomial expansion, although the situation is somewhat better in Fig. 5(B) than it is in Fig. 5(A). If a similar calculation were made with NACC, with coupling only of 0^+–2^+ state and using the potentials obtained by the power series expansion,[7] the results will further deviate from the solid curves than the dotted curves do in Fig. 5 and thus it is quite likely that conclusions obtained by fitting such theoretical results to experiments are misleading.

So far we have considered only protons as projectiles. In order to see how different results are expected if the projectile were neutrons, we made a calculation under the same condition as the solid curves of Fig. 5(B) were obtained, except that the charge of the projectile was put equal to zero. The results are shown in Fig. 5(C) and it is seen that they are quite different from the solid curves in Fig. 5(B). The very large oscillations in the elastic scattering cross section are remarkable. Also it is worthy of note that the 2^+ cross section is much larger than the corresponding one for the protons, which was perhaps caused by the fact that the nuclear and Coulomb interactions in V_{diag} are canceling each other when the projectile is charged. [No Coulomb excitation was included in Fig. 4(B), but its contribution was found to be very small in this case.]

We close this section by giving a remark concerning the magnitude of V_{so}. If it turns out that we can put $V_{so}=0$ without losing much accuracy of the result, we can perform the calculation for an incident nucleon by assuming that it is a spinless particle. If this can be done, it helps very much in saving the computational time as can be seen by comparing $N_c^{(n)}$ for $s=0$ and $s=\frac{1}{2}$ in Eq. (18) or observing Eq. (74). We have not yet made systematic calculations to see the dependence of various cross sections on V_{so}, but it was found that at least, when we consider scattering of nucleons of not too low energy by heavy and well-deformed nuclei, $V_{so}=0$ gives practically the same result as V_{so} of, say, 7.5 MeV does. Therefore the above-mentioned simplified calculation can be made in such cases, at least in the process of parameter searching.

Clearly, however, this argument does not apply to the discussion of the polarization. In fact in the calculation in which the solid curves of Fig. 5(B) were obtained (and thus $V_{so}=7.5$ MeV was used), the largest magnitudes of the polarization predicted theoretically in the 0^+, 2^+, and 4^+ state scattering were 0.2, 0.6, and 0.3, respectively.

VII. COMPARISON OF THE THEORETICAL RESULTS WITH EXPERIMENTS

We now proceed to the discussion of fits so far obtained and the information about the properties of target nuclei derived from such analyses.

A. Scattering by Even Vibrational Nuclei

In this category we have so far analyzed the data of the scattering or protons by ^{62}Ni, ^{64}Ni, ^{114}Cd, and ^{126}Te. We summarize the result here in the chronological order with which these analyses were made.

1. *Scattering of* 11-*MeV protons by* ^{62}*Ni and* ^{64}*Ni*[8]

The experimental data were obtained by Dickens, Perey, and Silva and the calculation was made by Perey and Tamura. The experimental differential cross sections to the one-phonon 2^+ and two-phonon 0^+, 2^+, and 4^+ states, and their corresponding theoretical curves are given in Fig. 6, and as is seen the agreement

TABLE II. Parameters of the analyses of scattering of protons by ^{62}Ni, ^{64}Ni, and ^{114}Cd.

Target	E_p (MeV)	V (MeV)	W_D (MeV)	One-phonon states Q(MeV)	I^π	β_2	Two-phonon states Q(MeV)	I^π	β_2	Reduction factor of $B(E2)$
							−2.05	0^+	0.170	0.36
^{62}Ni	11.00	50.84	10.21	−1.17	2^+	0.281	−2.30	2^+	0.230	0.67
							−2.34	4^+	0.281	1.00
							−2.28	0^+	0.170	0.54
^{64}Ni	11.00	51.23	11.51	−1.34	2^+	0.231	−2.62	4^+	0.231	1.00
							−2.89	2^+	0.189	0.67
							−1.15	0^+	0.130	0.42
^{114}Cd	12.16	48.8	12.20	−0.556	2^+	0.200	−1.21	2^+	0.172	0.74
							−1.28	4^+	0.164	0.67

between them are quite good, though not perfect. The finding of the set of parameters was made in the way explained in Sec. VI(ii), and we shall not repeat here. The parameters used in the final 0^+–2^+–0^+–2^+–4^+ coupling calculation with RFF were those of (75) and those summarized in Table II, where corresponding values for ^{114}Cd are also given.

The correspondence of the β_2 values given in Table II and those that appear in the expressions for the β matrices of Sec. III is clear. Thus the β_2 values that appear under the heading of "one-phonon state" in Table II are those that were assigned to the β_λ that appears in (36.1) with $\lambda=2$. The β_2 values that appear under the heading of "two-phonon states" are those

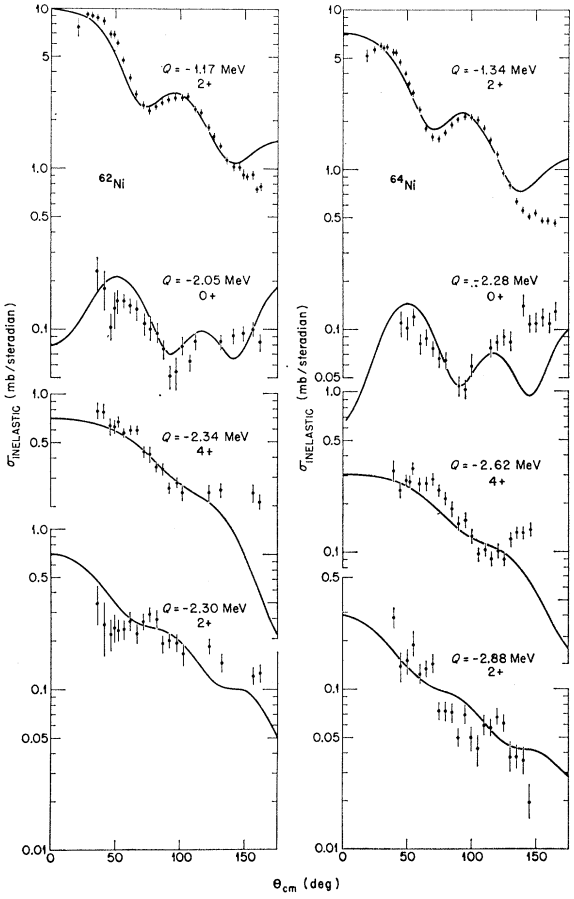

FIG. 6. Comparison with experiment of the result of the coupled-channel calculation of the scattering of 11-MeV protons by ^{62}Ni and ^{64}Ni. Parameters used are given in Table II.

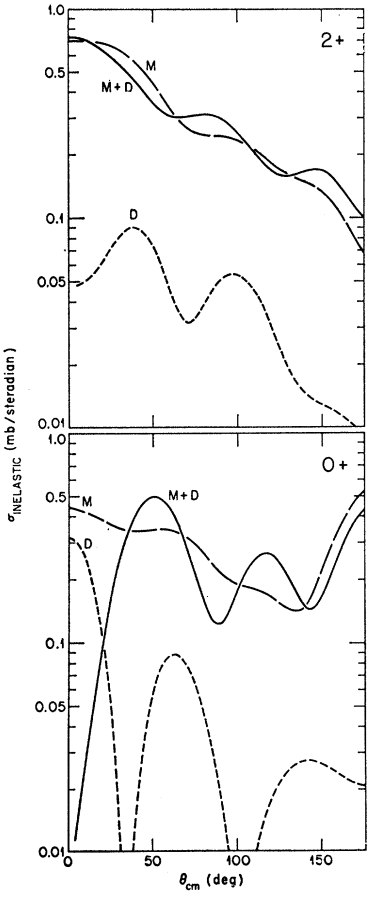

FIG. 7. Comparison of the contributions of direct (D) and multipole (M) processes of the excitation of the two-phonon 2^+ and 0^+ states in ^{62}Ni.

assigned to β_2 that appear in (36.2), where the spin I in (36.2) and in Table II correspond to each other. The fact that these β_2 values can depend on I and its physical significance have already been discussed in Sec. VI(ii).

There is another place where β_2 values appear in the coupling matrices. Namely, there are β_2's that originate from (37.1), which again can be functions of I. In order to keep the number of free parameters as small as possible, however, we put them equal to their corresponding values of β_2 of (36.2). This may cause some ambiguity in the interpretation of our analysis. Fortunately, however, there is a reason[8] to believe that the final result of the calculation does not depend very strongly on the β_2's of (37.1).

We show in the upper half of Fig. 7 the theoretical cross sections to the two-phonon 2^+ state of ^{62}Ni. The curve M (which stands for the multiple process) is the result obtained by putting β_2 of (37.1) equal to zero, while the curve D (which stands for the direct process) is the result obtained by putting β_2 of (36.2) equal to zero. As is seen, D is much smaller than M and this fact shows that the slight change of β_2 of (37.1) does not affect drastically the final result, $M+D$, which is obtained by using nonvanishing β_2 both in (36.2) and (37.1). [However, (37.1) cannot completely be neglected, because the M and D terms interfere with each other as is seen from the shift of the peaks and valleys between the curves M and M+D in Fig. 7.]

A similar situation was observed in a calculation that lead to the 4^+ state. The situation is somewhat different, however, when the 0^+ state is concerned. As is seen in the lower half of Fig. 7, the D cross section is rather large at least in the forward angles, and as a consequence the $M+D$ curve has a sharp dip in the forward angle which did not exist in the M curve.

The interference effect of the M and D terms were already discussed by Buck[6] in the excitation of the two-phonon 4^+ state of ^{58}Ni in the (α, α') process. In that case, however, the D cross section itself was as large as the M cross section, in contrast to the above mentioned (p, p') results for the 2^+ and 4^+ states.

The origin of this difference may be traced back to the differences in the absorption of protons and α-particles.[8] If we restrict ourselves for simplicity to RFF, the radial form factors of the M- and D-coupling terms are given by the first terms of (13.1) and (13.2), respectively; and while the former has a definite sign in the whole range of r, the latter changes its sign at $r=R_0$. Therefore, the radial matrix element of the M term can be much larger than that of the D term, if the wavelength of the projectile is sufficiently large and its absorption is not too strong, so that its amplitude is effectively constant within the range of r in which the above form factors have nonvanishing values. The above requirement is satisfied by protons of moderate energy and this explains the result observed in the upper part of Fig. 7. On the other hand, the α particles feel (because of the strong absorption) only the tails of the above form factors which are more or less of the same order of magnitude with each other. Therefore the D cross section can become as large as the M cross section. The fact that the forward D cross section is large in the excitation of the 0^+ states in the (p, p') process is understood in the same way, since for the zero angular momentum transfer in the forward angles, the peripheral scattering is dominant and in this case only the tails of the two form factors are felt by the protons. Whether the forward dip as seen in the $M+D$ curve for 0^+ state in Fig. 7 will appear or not depends on the energy of the protons and the target size, since it is an interference effect. Under favorable conditions that it does appear, however, it could be used in identifying the two-phonon 0^+ state.

The reduction factors of $B(E2)$ values [cf. Sec. VI(ii)] obtained from the β_2 values of Table II are very interesting. They are given in the last column of Table II and they are seen to be consistent with the corresponding reduction factors known for the $B(E2)$ values observed in ^{114}Cd by the Coulomb excitation analysis.[31]

When the analysis of Fig. 6, was made, the spins of the two-phonon states were not known, but the knowledge of the above reduction factors, as well as that of the shape of the cross-section curves, made us dare to assign the spins that are given to these states in Table II. (Unfortunately, the shapes of the experimental cross-section curves to the 2^+ and 4^+ states do not differ very much from each other.) Shortly after our analysis was made, however, results of $(p, p'\gamma)$ experiments from ^{62}Ni and ^{64}Ni were reported by Sen Gupta and Van Patter,[33] who showed that our spin assignment was correct. This result meant that the coupled-channel analysis can not only supply the knowledge of the β values, but also be used sometimes in assigning spins to unknown states, and this experience encouraged us to perform similar calculations which were made afterwards.

One unsatisfactory thing concerning the β_2 values in Table II is that their absolute magnitudes are somewhat too large compared to those obtained from other sources.[34–36] As can be seen, for example, in Fig. 3 and in many other calculations presented below, it is seen that CFF usually gives larger inelastic cross sections (for a given β) than RFF does. The result of a CFF calculation made for the present case showed, however, that it gives smaller cross sections than RFF does. In other words we need even larger β values than

[33] A. K. Sen Gupta and D. M. Van Patter, Phys. Rev. **131**, 318 (1963); Bull. Am. Phys. Soc. **8**, 375 (1963).
[34] P. H. Stelson and F. K. McGowan, Nucl. Phys. **32**, 652 (1962).
[35] P. H. Stelson and F. K. McGowan, Phys. Rev. **110**, 489 (1958).
[36] H. Faraggi and J. Sandinos, Paper C7, "Symposium on Nuclear Spectroscopy with Direct Reactions," Argonne National Laboratory Report ANL-6848, 1964 (unpublished).

those given in Table II if we had used CFF. We do not yet know why this discrepancy between our β_2 and those of other sources occurred. In most of the other cases to be presented, the β values deduced from our analyses were consistent with those derived from other sources, in particular when our calculations are made with CFF.

2. *Scattering of* 12.16-*MeV protons by* ^{114}Cd [10]

The experimental data were supplied by Sakai[10] and Fig. 8 shows the spectrum of ^{114}Cd states, for which the angular distributions of the inelastically scattered protons are observed in this experiment. In this figure the states B and H are known as quadrupole and octupole one-phonon states, respectively, while states C, D, and E are known as triad states of two quadrupole-phonons.[81] The nature of the states F and G is not very clearly known, but they may be considered as quasi (or single) particle states. Concerning the last five states I through M, it is interesting to note that they are closely spaced to each other and that their mean energy 2.53 MeV is approximately equal to the sum of the energies of states B and H. It is, therefore, tempting to consider that at least some of them could be members of the five quadrupole–octupole two-phonon (QOTP) 1^-, 2^-, 3^-, 4^-, and 5^- states, that were considered in Eq. (34) with $\lambda_1=2$ and $\lambda_2=3$.

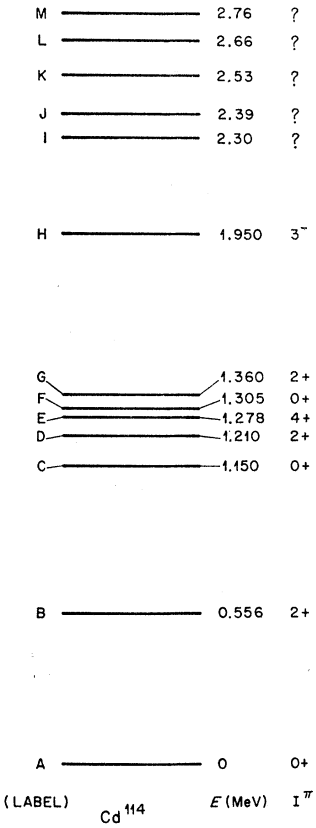

FIG. 8. Spectrum of ^{114}Cd states. All the states are labeled as A through M.

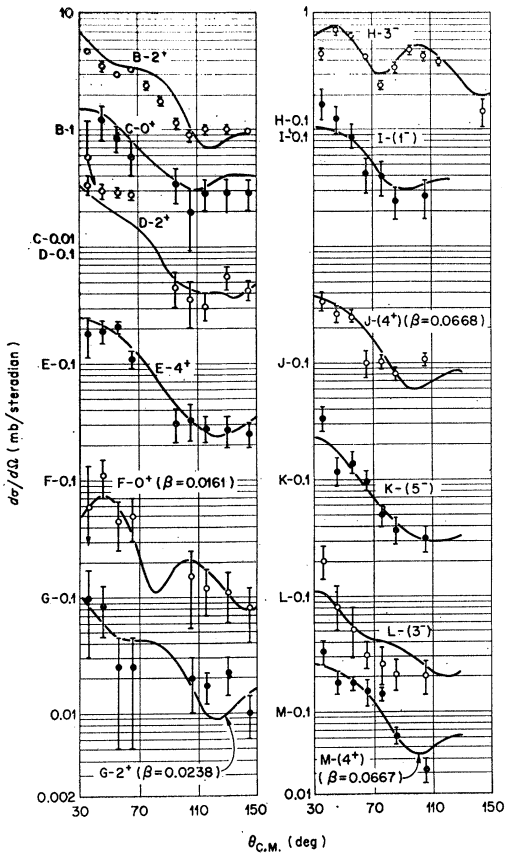

FIG. 9. Comparison of the theoretical and experimental differential cross sections of the scattering of 12.16-MeV protons by ^{114}Cd. The labelling of the curves corresponds to that in Fig. 8, and different scales used for different curves are labeled similarly.

We show that this idea is not inconsistent with the cross section data to these states.

As discussed in Sec. VI(iv), if all these states were coupled together, we would get a rather accurate result, but such a calculation is impossible. We therefore performed the calculation in the following way: (A) The states A, B, C, D, and E are coupled together: (B) The states A, B, H and one of the QOTP states are coupled together at one time: (C) The states F and G are coupled separately to A, assuming a very weak coupling parameter β_λ, the calculation thus giving essentially the same result as that of the DWBA[1]: (D) Similar DWBA-type calculations were made for 0^+, 1^-, 2^+, 3^-, 4^+, and 5^- states assuming an excitation energy of 2.53 MeV for all of them. In both (C)- and (D)-type calculations the radial part of the coupling term had the collective form factor as given in Eq. (13.1).

The type (A) calculation is exactly the same as we did for Ni isotopes in subsection (1) except that CFF is used rather than RFF this time. The optical model parameters, other than those in (75), and β_2 values used are again given in Table II and the theoretical cross sections obtained with these parameters

are compared with experiments in curves B through E in Fig. 9. The agreement is very good, except that the fit of curve B is somewhat poor.

In spite of this good agreement of the cross sections and the fact that β_2 values of Table II are of reasonable magnitude,[31] there is some unsolved problem concerning the reduction factors of $B(E2)$. As is seen in Table II, they are 0.42, 0.74, and 0.67 for 0^+, 2^+, and 4^+ states, respectively, which are to be compared with the corresponding values 0.43 ± 0.09, 0.61 ± 0.13, and 0.83 ± 0.11 obtained from the analysis of the Coulomb excitation experiment.[31] The two sets of reduction factors agree very well concerning the 0^+ state, while for the 2^+ state our value is barely within the error of the Coulomb excitation value. For the 4^+ state our value is definitely smaller than the Coulomb excitation value.

We have discussed in Sec. VI(iv) that it might be reasonable to use larger values of W_D for the highest energy states that are considered in the coupling, than its value used in the lower states. In the present calculation $W_D=12.2$ MeV as given in Table II was used in the ground and the first 2^+ state, but for the two-phonon states W_D was multiplied by a correction factor w_c which was equal to 1.2, 1.3, and 1.4, respectively, for 0^+, 2^+, and 4^+ states. The choice of these values were made rather arbitrarily, except that we cared to chose larger w_c for larger spin states motivated by the following reason: A higher-spin two-phonon state can be coupled with larger number of three-phonon states of higher spins, than a lower spin state can, and thus the neglect of such couplings to the three-phonon states could be treated by assigning a larger w_c to the former than to the latter.

If the ratio of w_c and β_2 [of (36.2)] is kept fixed, the cross section obtained is almost kept fixed. Therefore, if we had assumed a larger value of w_c to the 4^+ state than that was used above, we could have obtained a larger value of β_2 and in turn a larger reduction factor, in agreement with the result of the Coulomb excitation.

One can conceive of several reasons why the discrepancy, if any, of the reduction factors exists. As noticed in the end of Sec. VI, an improved analysis of the Coulomb excitation process is hoped to be made. It is desirable to redo our calculation by coupling the possibly existing three-phonon states. The absolute value of the 4^+ experimental cross section might be suspected. All these considerations clearly indicate that more work has to be done both experimentally and theoretically. The β_2 values deduced from the Coulomb excitation are those that describe the motions of the charge distributions, while our β_2 values are those of the whole nucleons, and thus they may not necessarily be needed to agree with each other. If it becomes definite that they are indeed different, it will give us an interesting new problem of nuclear structure theory.

The results of the (C)-type calculations made for the states F and G are shown as curves F and G in Fig. 9, and the good agreement seen there will mean that the assignment of the quasi-particle nature to those states was correct. The B_λ values used in the fit are 0.0161 and 0.0238, respectively, for states F and G, as are shown in the figure. Since the single-particle value β_{sp} of β for a pure single-particle transition may be estimated as $\beta_{sp}=0.0338$ [which equals $0.2/(35)^{\frac{1}{2}}$, where 0.2 is the β value of (36.1) while 35 is the enhancement factor of the $B(E2)$ value of the $0^+\rightarrow2^+$ transition as deduced from the Coulomb excitation experiment[31]], these transitions seem to be slightly inhibited compared to the pure single-particle transitions.

Through the type (D) calculation it is found that the states J and M are both consistent with the assignment of 4^+ quasi-particle states having some admixture of the hexadecapole-phonon state amplitude (since their β values are larger than β_{sp}), although 2^+ assignment to M may not be excluded. In the type (B) calculation it is found that 2^- and 4^- states are expected to be rather weakly excited and seem not to have been observed in this experiment, while the quantum numbers 1^-, 3^-, and 5^- could be assigned to the I, L, and K states, respectively. Comparison of the cross sections with experiments for states H through M is also made in Fig. 9, and the good agreement seems to support the above assignment of the nature and of the spin to these states. As was already remarked in Sec. VI(iv), the curve H in Fig. 9 is obtained in the 0^+–2^+–3^-–3^- calculation, where use is made of $\beta_2=0.2$ and $\beta_3=0.136$ all the way in Eqs. (36.1) (with $\lambda=2$ and 3), (36.4), (36.5), (37.3), and (37.4). The same values of β_λ were used in obtaining the curves K and L.

We used CFF throughout the calculations that lead to the curves of Fig. 9. If we had used RFF, we would have obtained cross sections that are smaller by factors of about 1.5. In other words, if RFF were used, we could not fit the data unless we used values of β_2 and β_3 which were larger than those used here. Since the present β values seem reasonable,[30,37] we may conclude that CFF is preferred to RFF.

We remarked in subsection (1) that the similarity of the experimental cross sections of the two-phonon 2^+ and 4^+ states made the definite assignment of these spins somewhat difficult. Similar problem appears here; see for example, the similarity of the cross sections to states I and L. Considering that a part of this difficulty could be removed if the same experiment were performed with a higher energy protons, we calculated the differential cross section for the QOTP 1^- and 3^- states both for $E_p=12.16$ and 40 MeV, using the same optical model parameters as given above but with RFF for all the cases, and the results are compared in Fig. 10. For $E_p=40$ MeV, a rather marked structure appears for the 1^- curve and the difference between the 1^- and 3^- curves seems to be

[37] See, e.g., G. R. Satchler, R. H. Bassel, and R. M. Drisco, Phys. Letters **5**, 256 (1963).

significant. These features suggest it would be worthwhile to perform such a high-energy experiment in the future, although a calculation made for $E_p=40$ MeV with the type-(A) coupling did not lead to as much structure in the angular distributions for the states C, D, and E.

3. *Scattering of 12-MeV protons by* ^{126}Te[11]

The experimental data were obtained by Pramila and Middleton[11] and the theoretical analysis was made by Satchler and Tamura.

The experimental cross sections to the one-phonon 2^+, two-phonon 2^+, and 4^+ states are shown in Fig. 11. A theoretical calculation was made by taking 0^+–2^+–0^+–2^+–4^+ coupling scheme and by using RFF, $V=53$ MeV and $W_D=12.4$ MeV. In every element of the coupling matrix $\beta_2=0.18$ was used. The result of this calculation is compared with experiment in Fig. 11, where the curves for the two 2^+ states are given in dotted lines. Although no state that could be assigned to the two-phonon 0^+ state was observed experimentally, the theoretical cross-section curve to this state (assumed to lie at 1.4 MeV) is shown in this figure. A calculation was also performed by considering only a 0^+–2^+–2^+ coupling, but taking into account the Coulomb excitation [cf. (13.1)], and the results to the two 2^+ states are given by full lines.

The over-all agreement with experiment shown in Fig. 11 is very satisfactory. The discrepancy at back angles for the two-phonon states may not be too

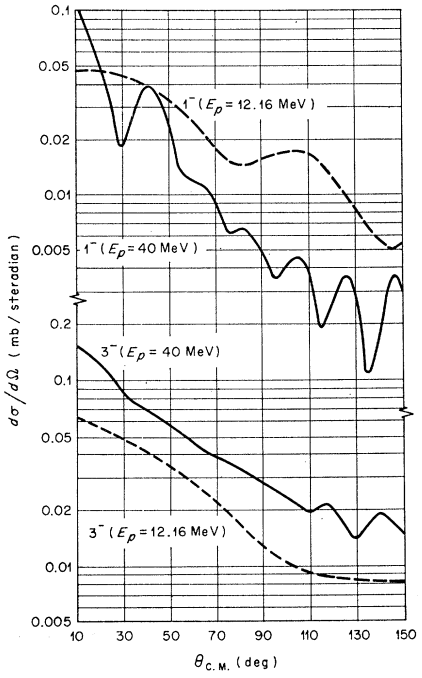

FIG. 10. Comparison of the theoretical differential cross sections for $E_p=12.16$ and $E_p=40$ MeV.

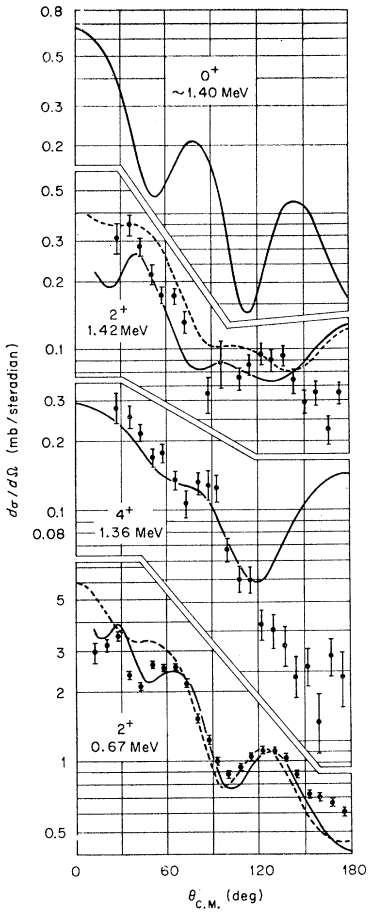

FIG. 11. Comparison of the theoretical and experimental differential cross sections of the scattering of 12-MeV protons by ^{126}Te. Full and dotted lines for 2^+ states are the results with and without Coulomb excitation, respectively.

important; the cross section here is known to be quite sensitive to small changes in parameters. The absence of the 0^+ state is puzzling; it does not seem likely that it is unresolved from either the 1.36- or 1.42-MeV group of the spectrum of the scattered protons because if it were it would severely modify the corresponding angular distribution and change the relative magnitude of these two groups. Although excitation of the corresponding 0^+ state in Cd and Ni isotopes was found to be somewhat inhibited, as was discussed in subsections (1) and (2), it was only by a factor two or so.

It is remarkable to see in Fig. 11 that the inclusion of the Coulomb excitation improves the fit to the two 2^+ state very much. Even the small oscillations that are seen in these cross sections at smaller angles are reproduced theoretically. Unfortunately the inclusion of the Coulomb excitation makes the machine time needed very long, since in that case we have to give very large values to $J_{\max}$ and R_m [(cf., text above Eq. (77)]. We therefore could not perform similar calculations when the larger number of states were coupled

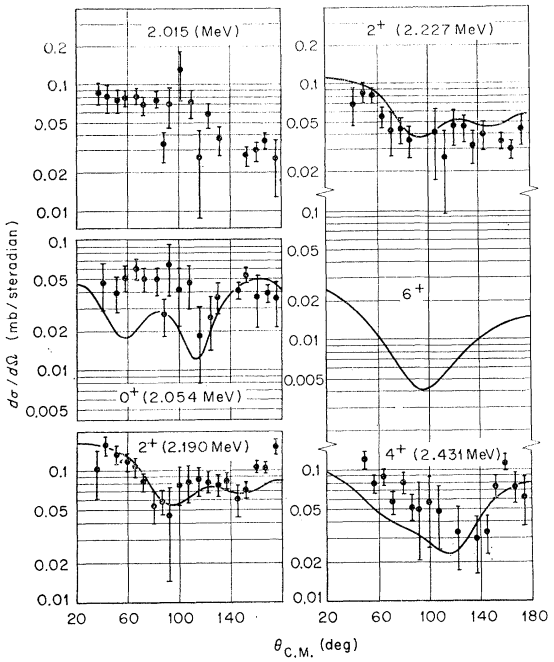

FIG. 12. Assignments of spins to possible three-phonon states in ^{126}Te.

together, but the effect is expected to be much less on the 4^+ excitation because the crossover transition is an $E4$ and the multiple-Coulomb-excitation effect is small.

In the experiment[11] a band of states were observed at about 2 MeV which were more weakly excited than those shown in Fig. 11. The angular distributions of five of these states are shown in Fig. 12. Since their mean energy (2 MeV) is close to three times the energy of the first 2^+ state, it is tempting to interpret at least some of these as members of the three-quadrupole phonon quintet (with spins 0, 2, 3, 4, 6, and even parity) expected at about this energy. Evidence has already been adduced[38] from γ decay for the existence of three-phonon states in the nuclei Pd, Cd, Xe, and Pt. Inelastic scattering could prove very useful in providing complementary evidence concerning the nature of these states. It is then of interest to calculate the differential cross sections for this quintet of states, and this was done using the same parameters as for the two-phonon calculation, but this time using CFF. The results are included in Fig. 12. The chief effect of switching from RFF to CFF is to increase the cross-section magnitude somewhat as was already remarked in subsection (a); the changes in angular distribution are insignificant in comparison to the experimental errors.

The coupling matrix elements in which three-phonon states are related are found in Eqs. (36.3) and (37.2). In order to make the calculation feasible, only one of the three-phonon states is taken as a coupled state each time and among the two-phonon states only those that are coupled directly to the concerned three-phonon state are included. Therefore the coupling considered were 0_0^+–2_1^+–2_2^+–0_3^+, 0_0^+–2_1^+–0_2^+–2_2^+–4_2^+–2_3^+, 0_0^+–2_1^+–2_2^+–4_2^+–3_3^+, 0_0^+–2_1^+–2_2^+–4_2^+–4_3^+, and 0_0^+–2_1^+–4_2^+–6_3^+, where the suffices show the number of phonons in each state.

Although definite theoretical curves have been associated with the four angular distributions of the experiment in Fig. 12, it is clear that the accuracy of the data does not allow unambiguous identification. This is emphasized by the fact that both the 2.19- and 2.227-MeV levels are condidates for the 2^+ assignment, and the same theoretical curve is shown for both angular distributions. Although, as mentioned above, the theoretical cross sections were originally obtained for $\beta_2=0.18$, those shown in Fig. 12 for the 2.054, 2.19, and 2.413 levels have been further increased by 30%. This is not serious when it is remembered that the three-phonon cross sections are roughly proportional to $\beta_\lambda{}^6$. The 3^+ cross section is very small (approximately 1 μb/sr and less) and is not shown in Fig. 12. This occurs because multiple excitation is much more important than direct transitions [cf. subsection (1)], and the 3^+ state can be excited via both the 2^+ and 4^+ members of the two-phonon triplet. These two contributions to the amplitude, however, have opposite signs and produce considerable cancellation; (cf. the $I'=3$ column of Table IB). The 6^+ state is also predicted to be rather weak, and cannot be identified in this experiment. It would be valuable to have more precise data in this region of excitation.

B. Scattering by Deformed Nuclei

1. *Scattering of 17.5-MeV Protons by ^{165}Ho and ^{156}Gd*

The experimental data shown in Fig. 13 are those that were given by Lieber and Whitten.[39] The theoretical analysis was first made by performing NACC calculations,[9] but we now know that ACC gives results more accurate than NACC does as was discussed in Secs. V and VI(v). Therefore we show only the comparison of the ACC result with experiment.

The curves shown in Fig. 13 are similar to those that were shown in Fig. 4 as dotted lines except that now CFF is used, and thus need not be explained anew [cf. Sec. VI(v)]. The agreement of these curves with experiment is very good, considering the fact that there were essentially no free parameters in our calculation in the sense that the standard parameters (75) and $V=50$ MeV and $W_D=7.5$ MeV were used together with $\beta_2=0.30$ and 0.32, respectively, for ^{165}Ho and ^{156}Gd, which were already known from other

[38] Y. Yoshizawa, Phys. Letters **2**, 261 (1962).

[39] A. Lieber and C. A. Whitten, Phys. Rev. **132**, 2582 (1963).

sources.[40,41] With these parameters RFF gives inelastic cross sections that are somewhat too small. [The disagreement of the inelastic cross sections seen in Fig. 13 at smaller angles is probably due to insufficient unfolding of the contribution from the tail of the elastic scattering,[39] and so is not serious. The disagreement of the 0^+, 2^+ (and 5^+) cross sections of ^{156}Gd at $\theta=110°\sim130°$ is somewhat disturbing. The reason for this disagreement may be due to unsuspected experimental errors, although the authors of Ref. 39 feel this is unlikely.[42]]

2. *Scattering of 350-keV Neutrons by ^{165}Ho*

The experiment was performed by Wagner, Miller, and Marshak[12,43] and a remarkable feature in it is that part of this experiment was made by using a polarized target. The analysis of this experiment was the reason why we had to write down explicitly the lengthy formulas in Sec. IV, by introducing the amplitudes $a_{m_s}^{(i)}$ and $b_{M_1}^{(i')}$.

We first made the analysis of the differential cross section $\sigma(\theta)$ of the elastic scattering of unpolarized neutrons by an unpolarized target. Since the energy of the neutrons is low the theoretical cross section is now the sum of $\sigma_1^{(s)}(\theta)$ and $\sigma_1^{(c)}(\theta)$, given, respectively, by (47) and (57), contrary to the preceding calculations in which (57) could be neglected. The result is to be compared with the experimental result given in Fig. 14. Since the target is not yet oriented we can use (62) and (61) for the amplitudes $a_{m_s}^{(i)}$ and $b_{M_1}^{(i')}$ just as was done in the preceding calculations. In spite of the large deformation of ^{165}Ho, we used NACC contrary to the preceding subsection, because the energy of the neutron was low.

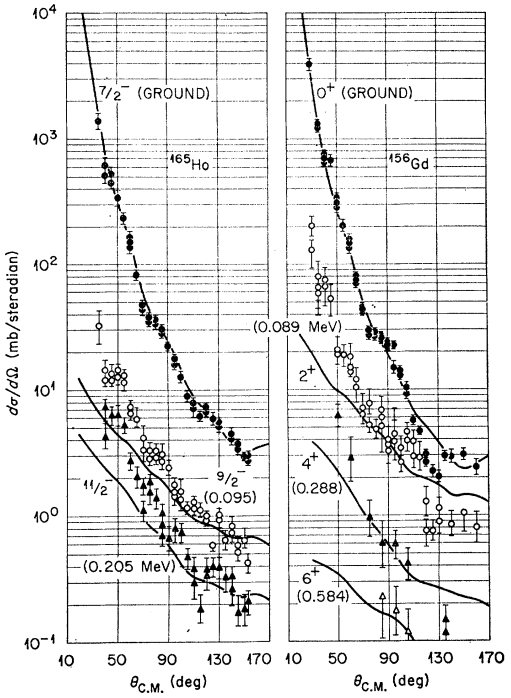

FIG. 13. Comparison of the ACC calculations of the scattering of 17.5-MeV protons by ^{165}Ho and ^{156}Gd with experiments.

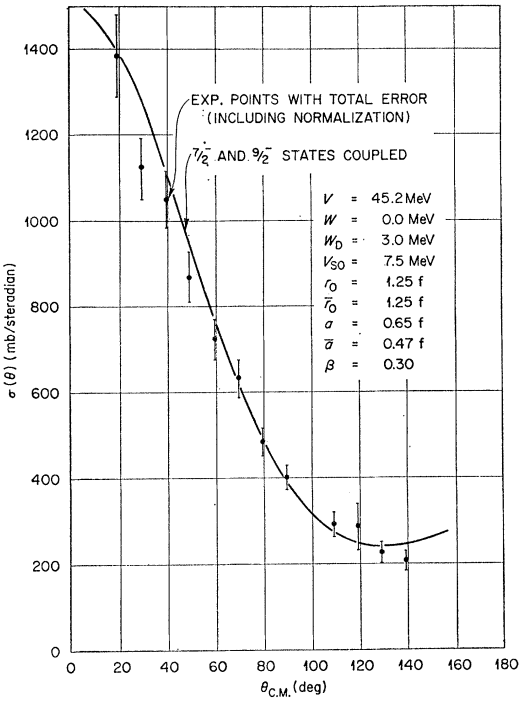

FIG. 14. Comparison of the theoretical and experimental cross section of the elastic scattering of 350-keV neutrons by ^{165}Ho.

With calculations made using (75) and $V\approx45$ MeV, $W_D\approx3$ MeV, the following features were found. (A) with $\beta=0$ (which is the uncoupled optical-model calculation), the theoretical $\sigma(\theta)$ is too small for small θ and too large for large θ. (B) When β_2 is taken as 0.3 [cf. subsection (1)], but only the partial waves belonging to the $7/2^-$ ground-state channel are coupled, the situation becomes better. Still the difficulty met with in (A) is not completely removed. (C) If furthermore the partial waves which belong to the first excited $9/2^-$ state channel are coupled (an approximation which may be called two-channel coupling), the *shape* of the theoretical $\sigma(\theta)$ agrees well with experiment, though not necessarily the magnitude.

These features clearly indicate the importance of the coupled-channel calculation, with at least two channels being coupled. We therefore made within the

[40] E. G. Fuller and E. Hayward, Nucl. Phys. **30**, 613 (1962); M. Danos and W. Greiner, Phys. Letters **8**, 113 (1964); E. Ambler, E. G. Fuller, and H. Marshak (to be published).

[41] B. Elbek, *Determination of Nuclear Transition Probabilities by Coulomb Excitation* (Ejnar Munksgaards Forlag, Copenhagen, Denmark, 1963).

[42] A. Lieber (private communication).

[43] R. Wagner, P. D. Miller, T. Tamura, and H. Marshak, Phys. Rev. **139**, B29 (1965).

framework of two-channel coupling a fairly extensive survey of the parameters V and W_D, and also of $\bar{r}_0$ of (75), as summarized below.

In the course of our calculation we also calculated σ_t, the total cross section [cf. Eq. (53)] for an unpolarized beam and unpolarized target, and it was found that σ_t is a very sensitive function of V for each set of fixed values of W_D and $\bar{r}_0$. Utilizing this fact it was then always possible to find a value of V for a fixed set of W_D and $\bar{r}_0$ so as to get exact agreement of σ_t with its experimental value, $\sigma_t^{(\mathrm{exp})}=7.94$ b. It is also found that $\sigma(\theta)$ is in good agreement with experiment not only in shape but also in magnitude when the relation $\sigma_t=\sigma_t^{(\mathrm{exp})}$ is achieved. In other words we can find a number of sets of V, W_D, and $\bar{r}_0$ that give the measured values for σ_t and $\sigma(\theta)$.

We now turn to the calculation of the cross sections from polarized targets. In order to be able to perform such calculations, however, we have to know the state of polarization of the target, or have to establish a definite model so that we can write down the coefficients $b_{M_1}{}^{(i')}$ explicitly. The derivation of such a model has been discussed in detail in our previous paper.[43] Here we give only a brief description of the model which was used in our coupled-channel calculation.

The holmium target used was in the form of a metal single crystal. It consists of two domains α and β if a moderately strong magnetic field is applied to it in its basal plane. The nuclei in the α domain are all polarized in the direction of the applied magnetic field, while those in the β domain are separated into six equally populated groups. All the directions of the polarization of these six groups of nuclei also lie in the basal plane and make an angle of 60° with each other. It is thus clear that the nuclei in the β domain give vanishing polarization. In other words only the α domain contributes to the nonvanishing polarization or the magnetization of the holmium crystal. The weight (or the fraction) of the α domain was 0.19 when the applied magnetic field was 10 kOe and the temperature was 0.34°K, under which the experiments were performed.

The experiment was made with the geometry so that the direction of the incident beam, which was taken as the z axis in Sec. IVD is perpendicular to the basal plane. Let us then take the positive x axis in the direction of the external magnetic field which is nothing but the direction of polarization of the α domain and thus can be identified with the z' axis (for the α domain) also introduced in Sec. IVD. If this choice is made the Euler angles (θ_i) introduced in Eq. (60) become as $(0, -90°, 0)$. If the z' axis is taken in the direction of the negative x axis (θ_i) become as $(0, 90°, 0)$. The Euler angles corresponding to the six groups of the β domain become more complicated, but we shall show below that for our present purpose we do not need to know these Euler angles.

Since (θ_i) are thus given, our knowledge needed in describing $b_{M_1}{}^{(i')}$ is completed if the occupational probabilities $P(N_1)$ introduced in Eq. (58) are given. They were found to have the values as given in Table III, under the 10-kOe external magnetic field and the temperature of 0.34°K.

Two experimental quantities were obtained by using this polarized target. They were the total cross sections of the 350-keV neutrons which was polarized by 55% in the direction of the positive x axis [i.e., $P=55$ in Eq. (63)]. The target was polarized once in the direction of the positive x axis and in another case in the negative x axis. Let us call the total cross sections thus obtained as $\sigma_t{}^{\uparrow\uparrow}$ and $\sigma_t{}^{\uparrow\downarrow}$, respectively. Their difference, which we shall call the experimental polarization effect and denote as $\sigma_{\mathrm{pol}}{}^{(\mathrm{exp})}$ was observed as[12,43]

$$\sigma_{\mathrm{pol}}{}^{(\mathrm{exp})}\equiv\sigma_t{}^{\uparrow\uparrow(\mathrm{exp})}-\sigma_t{}^{\uparrow\downarrow(\mathrm{exp})}=30\pm85\ \mathrm{mb}. \quad (78)$$

If the total cross section for the unpolarized target $\sigma_t{}^{(\mathrm{exp})}$ given above is subtracted from the mean value of $\sigma_t{}^{\uparrow\uparrow(\mathrm{exp})}$ and $\sigma_t{}^{\uparrow\downarrow(\mathrm{exp})}$, we get a quantity $\Delta\sigma_{\mathrm{def}}$ (which we shall call the deformation effect) and its experimental value was found to be[12,43]

$$\Delta\sigma_{\mathrm{def}}{}^{(\mathrm{exp})}=350\pm100\ \mathrm{mb}. \quad (79)$$

We start with the calculation of the deformation effect: $\Delta\sigma_{\mathrm{def}}{}^{(\mathrm{th})}$. Since $\sigma_{\mathrm{pol}}{}^{(\mathrm{exp})}$ is small as is seen in (78) and consequently the spin–spin interaction which is introduced below is also small, we shall neglect the latter at this stage. (Then theoretically $\sigma_t{}^{\uparrow\uparrow}=\sigma_t{}^{\uparrow\downarrow}$.) Considering this fact and the fact that all the nuclei, both in the α and β domains are polarized (or rather oriented) in the basal plane while the incident beam is perpendicular to this plane, it is easy to see that the nuclei in the α domain and the six groups of the β domain contribute to the total cross section simply in proportion to their weight. In other words we can get accurate $\Delta\sigma_{\mathrm{def}}{}^{(\mathrm{th})}$ by subtracting σ_t from the total cross section obtained by assuming that there were only α domain with weight unity and thus no β domain. Clearly this latter cross section, $\sigma_t{}^{(\mathrm{pol})}$, is obtained from (53) by using $b_{M_1}{}^{(i')}$ of (60) with $(\theta_i)=(0, -90°, 0)$ and P_{N_1} of Table III. [The result does not change even if $(\theta_i)=(0, 90°, 0)$ is used, since $\sigma_t{}^{\uparrow\uparrow}=\sigma_t{}^{\uparrow\downarrow}$. The result is also independent whether we use (62) or (63) with $P=55$ for $a_{m_s}{}^{(i)}$.]

We mentioned before that there are many sets of V, W_D, and $\bar{r}_0$ which give $\sigma(\theta)$ and σ_t that agree with experiment. In the course of obtaining such sets, we also computed $\sigma_t{}^{(\mathrm{pol})}$ and it was found that it is also a sensitive function of V for a fixed set of W_D and $\bar{r}_0$, just as σ_t was, but the difference $\Delta\sigma_{\mathrm{def}}{}^{(\mathrm{th})}=\sigma_t{}^{(\mathrm{pol})}-\sigma_t$

TABLE III. Population numbers of the nuclear magnetic substates for ^{165}Ho.

N	$+\frac{7}{2}$	$+\frac{5}{2}$	$+\frac{3}{2}$	$+\frac{1}{2}$	$-\frac{1}{2}$	$-\frac{3}{2}$	$-\frac{5}{2}$	$-\frac{7}{2}$
P_N	0.587	0.241	0.097	0.039	0.015	0.006	0.003	0.001

is rather insensitive to V. The value of $\Delta\sigma_{\rm def}^{\rm (th)}$, however, varies from one set of W_D and $\bar{r}_0$ to another. Thus, it is possible to discriminate between sets of values of V, W_D, and $\bar{r}_0$ by comparing $\Delta\sigma_{\rm def}^{\rm (th)}$ with experiment, a feature which the consideration of only σ_t and $\sigma(\theta)$ did not have. In Fig. 15 we plot $\Delta\sigma_{\rm def}^{\rm (th)}$ as a function of $\bar{r}_0$ for values of $W_D=3$ and 5 MeV, where the value of V has always been taken so as to satisfy $\sigma_t=\sigma_t^{\rm (exp)}$. Since the shaded area in this figure indicates the experimental value of the deformation effect (79), it is seen that if $W_D=3$ MeV is used, one gets very good agreement with the measured $\Delta\sigma_{\rm def}^{\rm (exp)}$ for any value of $\bar{r}_0$ ranging from 1.25 to 1.45 F. On the other hand, if $W_D=5$ MeV is used, the theory predicts too small a value of $\Delta\sigma_{\rm def}^{\rm (th)}$, and thus this value of W_D can be excluded.

The theoretical angular distribution of the elastically scattered neutrons was calculated using a set of parameters that gave good agreement with the experimental values of σ_t and $\Delta\sigma_{\rm def}$, namely, (75), $V=45.18$ MeV and $W_D=3$ MeV. In Fig. 14 the result is compared with the experiment, and it is seen that very good agreement was obtained.

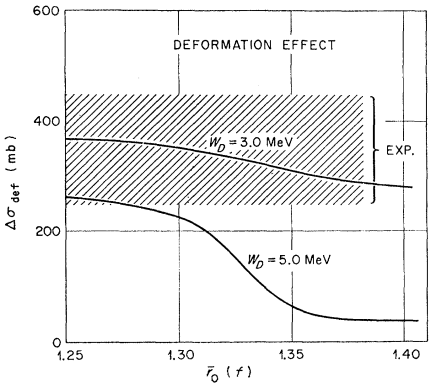

FIG. 15. Comparison of the theoretical and experimental deformation effects.

Using the same parameters as in Fig. 14, we also computed σ_t for E_n, the neutron energy, ranging from 290 to 420 keV, and the results are in good agreement with experiment, as is seen in Fig. 16.

Having established a satisfactory set of parameters we turn to the calculation of the polarization effect. In order to study this effect, we first introduce a spin–spin interaction of the following form[44]:

$$-V_{ss}(\boldsymbol{\sigma}\cdot\mathbf{I})(1+e)^{-1}, \tag{80}$$

where I is the spin operator for the target state, while e was defined in Eq. (4). The matrix element of (80), which is given by

$$-V_{ss}(1+e)^{-1}\,\delta_{II'}\,\delta_{ll'}[6I(I+1)(2I+1)]^{\frac{1}{2}}$$
$$\cdot\hat{j}\hat{j}'(-)^{J+j+j'+\frac{1}{2}+l-I}W(\tfrac{1}{2}\tfrac{1}{2}jj';1l)W(JIj'I';J1), \tag{81}$$

is to be added to (40) in solving the coupled equations (25).

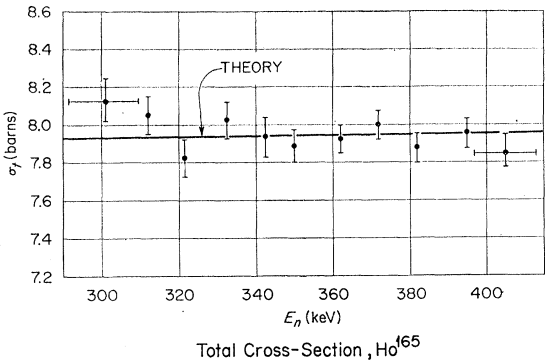

FIG. 16. Comparison of the theoretical and experimental total cross sections of neutrons by ^{165}Ho as a function of the neutron energy.

From Eqs. (78) and (80), and from the fact that the β domain has zero net polarization, it is easy to see that only the α domain contributes the polarization effect. In other words, we add (81) to (40), calculate σ_t of (53) by using $b_{M_1}^{(i')}$ of (60) with $P(N_1)$ of Table III, and one time with $(\theta_i)=(0,\,-90°,\,0)$ and the other time with $(\theta_i)=(0,\,90°,\,0°)$. Then we take the difference of the two total cross sections thus obtained and finally multiply it by 0.19, which is the weight of the α domain. Of course one has to use (63) for $a_{m_s}^{(i)}$ with $P=55$.

The theoretical $\sigma_{\rm pol}^{\rm (th)}$ thus obtained is plotted in Fig. 17 as a function of V_{ss}. Since the corresponding experimental value 30 ± 85 mb is expressed by the shaded area of that figure we can conclude that the possible values of V_{ss} satisfy the following inequality;

$$-130\text{ keV}<V_{ss}<280\text{ keV}. \tag{82}$$

Thus it is seen that the spin–spin interaction is more than one order of magnitude smaller than the spin–orbit interaction.

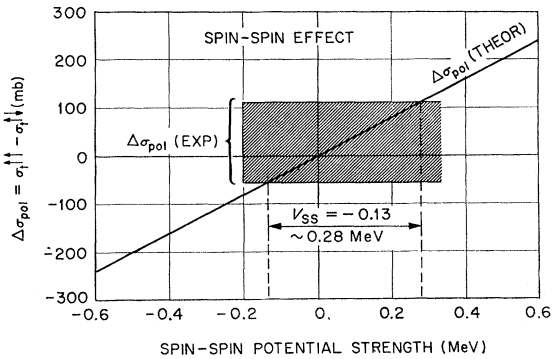

FIG. 17. Determination of the strength of the spin–spin interaction through comparison of the theoretical and experimental polarization effects.

[44] K. T. R. Davies and G. R. Satchler, Nucl. Phys. **53**, 1 (1964).

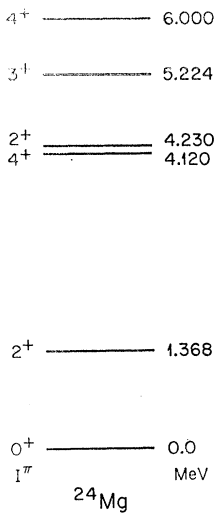

FIG. 18. Spectrum of ^{24}Mg states.

3. *Scattering of 28.5-MeV α particles by ^{24}Mg*

So far we considered nucleons exclusively as projectiles, but here we shall give an example of the scattering of α particles. The data were those of Kokame *et al.*,[45] and Fig. 18 shows the spectrum of the states of ^{24}Mg for which scattering data were obtained.

Since the detail of this calculation has been reported elsewhere,[46] we shall simply summarize the result here. Among the states of Fig. 18 the lowest three would be members of the $k=0$ rotational band, while the other three would be members of the γ-vibrational $k=2$ band.

If we take this interpretation, we have to extend the first equation of (3) by adding $R_0\beta\gamma 2^{-\frac{1}{2}}(Y_{22}(\theta',\phi')+Y_{2-2}(\theta',\phi'))$ on the right-hand side so that the excitation of the γ-vibrational state is described.[19] (We put $W_D=0$ for α particles.) Equation (1) with this modified Eq. (3) is then expanded in powers of γ (to the first order in γ) and then the coefficients are further expanded in terms of the Legendre polynomials in a way similar to that made in (16). The interaction potential (15) and the coupling matrix (40) are modified accordingly, and the new matrix elements that are to be added to (40) are proportional to γ_0, the zero-point amplitudes of the γ vibration, which becomes a new parameter. When γ vibration is considered, ACC can no longer be used and the whole calculation has to be made with NACC.

The result is compared with experiment in Fig. 19, the over-all agreement is very satisfactory. In particular the agreement of the 0_0^+ and 2_0^+ (the suffices meaning the K quantum number) cross section is almost perfect except at angles larger than, say 85° in the former and 75° in the latter. The theoretical $4_0^+ + 2_0^+$ cross sections have a pattern close to that of the experiment though the former is slightly rotated from the latter counterclockwise. The 3_2^+ cross section (solid line) has a phase opposite to that of experiment at larger angles, but the agreement at $\theta \leq 60°$ is very good. The experimental error quoted in Fig. 19 is only statistical. If the systematic errors were also added, the total experimental error must have been much larger, at least for the higher excited states.

The parameters that were used in this calculation were the following:

$$\begin{aligned} &V=54.4 \text{ MeV}, && W=5.6 \text{ MeV}, \\ &a=0.413 \text{ F}, && a_w=0.405 \text{ F}, \\ &r_0=1.76 \text{ F}, && r_w=1.80 \text{ F}, \\ &\beta=0.34, && \gamma_0=0.62 \text{ (rad)}. \end{aligned} \tag{83}$$

As is seen the imaginary part of the optical model potential is assumed to have the Saxon-shape (not its derivative) and the diffuseness parameter a_w and the radius parameter r_w for this imaginary part were taken somewhat differently from a and r_0.

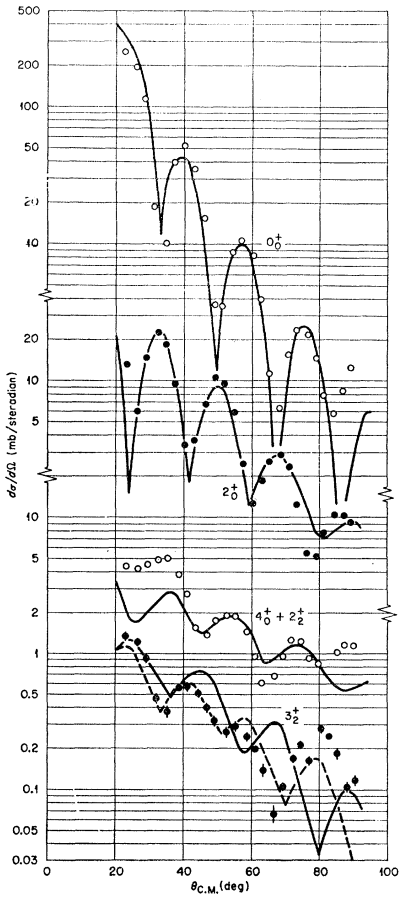

FIG. 19. Comparison of the theoretical and experimental cross sections of the scattering of 28.5-MeV α particles by ^{24}Mg.

[45] K. Kokame, K. Fukunaga, N. Inoue, and H. Nakamura, Phys. Letters **8**, 342 (1964); K. Kokame (private communications).

[46] T. Tamura, Nucl. Phys. (to be published).

The coupling scheme considered in the calculation was 0_0^+–2_0^+–4_0^+–6_0^+–2_2^+–3_2^+. The addition of the 6_0^+ state (assumed to lie at 9.0 MeV) was needed to give accurate cross section to the 4_0^+ state [cf. Sec. VI(v)].

There is some reason[45] to suspect that the experimental 3_2^+ cross section shown in Fig. 19 is given a little too large absolute value than it actually has, and thus that the corresponding theoretical cross section is to be multiplied by a factor which is larger than unity, before it is compared with experiment. We took this factor, somewhat arbitrarily, as 2 and thus the theoretical 3_2^+ curve in Fig. 4 has twice the magnitude of the computed cross section. If this manipulation is indeed allowed, the good agreement obtained in Fig. 4 leads us to conclude that the multiple excitation process, which is embodied in our coupled-channel calculation, does explain the excitation in the (α, α') process of the unnatural parity states[47] not only qualitatively but also quantitatively.

However, the agreement in shape achieved by the solid curve for the 3_2^+ cross section in Fig. 19 is not necessarily very good at larger angles, as was noticed above. Since the explanation of this cross section had been the primary purpose of the present analysis, we thought it worthwhile to seek for another set of parameters [other than that of (83)], which gives better agreement to this cross section, although the agreement to the cross sections to other states may be worsened in this way. The dotted curve shown in Fig. 4 is the result (times 2) of a run in which $r_v = r_w = 1.94$ F was used, other parameters being the same as in (21). As is seen, the agreement is now almost perfect, even the small hump at $\theta \approx 55°$ being reproduced.

VIII. DISCUSSIONS AND CONCLUSIONS

As we have seen in Sec. VII, coupled-channel calculations give very good agreement with a number of existing experimental data. It is gratifying to know that such good agreements were obtained (when nucleons are used as projectiles) by using optical-model parameters that are (almost) independent of mass numbers and the types of the targets. The values required for β_λ that describe the collectivity associated with the excitation of various states were also found quite reasonable. These results indicate that the inelastic, as well as elastic, scattering experiment and its analysis in terms of the coupled-channel calculation provides a powerful tool in investigating the spectroscopic properties of various states in collective nuclei.

This sort of analysis sometimes allows us to assign spins to states for which they were unknown beforehand, as for example, were made for ^{62}Ni, ^{64}Ni, ^{114}Cd, and ^{126}Te. Although such assignments of the spins and the interpretations of the properties of those levels may not always be taken too seriously at the present time, if some complementary experiments, such as β–γ spectroscopy, $(p, p'\gamma)$ correlation experiment and so forth were performed for those nuclei, we would have a very clear understanding of the properties of these (collective) states. Such combined experiments would be very welcome.

Although we have made so far a fairly large number of calculations, many more interesting problems could be analyzed by using our code. Experiments which excite higher phonon states in vibrational nuclei, intrinsic states in deformed nuclei (in particular β and γ vibrational states), and states in transitional nuclei are quite interesting [cf. Sec. VI(i)]. Certainly data for the scattering obtained by using α particles and deutrons as projectiles will also be of interest. In fact several analyses of this sort have been reported, although so far they have been limited to the excitation of one or two lower excited states.[6,29,48] (See, however, Sec. VIIB3). {*Note added in proof.* Recently an analysis of ^{60}Ni$(d,d')^{60}$Ni* processes was made with the 0–2–0–2–4 coupling (vibrational nucleus) and it was found that deuteron is a very useful probe for our purpose [T. Tamura and R. K. Jolly, Phys. Letters (to be published)].}

In order to be able to analyze experimental data which have been and will be accumulated rapidly, it is desirable to know more systematically the behavior of the cross sections as functions of various parameters and coupling schemes. In other words the sort of calculations as exemplified in Sec. VI have to be made more systematically and more extensively.

Modifications of the way of calculation should also be tried in order to increase the flexibility in data fitting. For example, it may be desirable, if possible, to use wave functions for the collective state, not described phenomenologically as were made in the present paper, but derived from first principles.[49]

Even using the phenomenological description, however, there are ways to improve the present scheme of the calculation. For example, for vibrational nuclei we used for the wave functions of their states those which are correct only for ideally harmonic vibrational nuclei, i.e., (33), (34), etc. of Sec. III, and in order to describe the deviation from the harmonicity, we simply made β_λ adjustable parameters.

One of the possible ways to improve such a situation would be to describe various states as linear combinations of the wave functions of the ideal vibrational states. We show in Fig. 20 the result of a preliminary analysis of the scattering of 17.5-MeV protons by ^{64}Zn. The data were given by Roberson[50] and our theoretical result for a 0^+–2^+–2^+–4^+ (and of a 0^+–2^+–3^-) calculation are given by solid lines.

In obtaining these curves the wave function of the

[47] W. W. Eidson and J. G. Cramer, Jr., Phys. Rev. Letters **9**, 497 (1962).

[48] T. A. Belote, J. H. Bjerregaard, O. Hansen, and G. R. Satchler (to be published).

[49] See, e.g., T. Tamura and T. Udagawa, Nucl. Phys. **53**, 33 (1964) and the other works cited in this paper.

[50] N. R. Roberson (private communication).

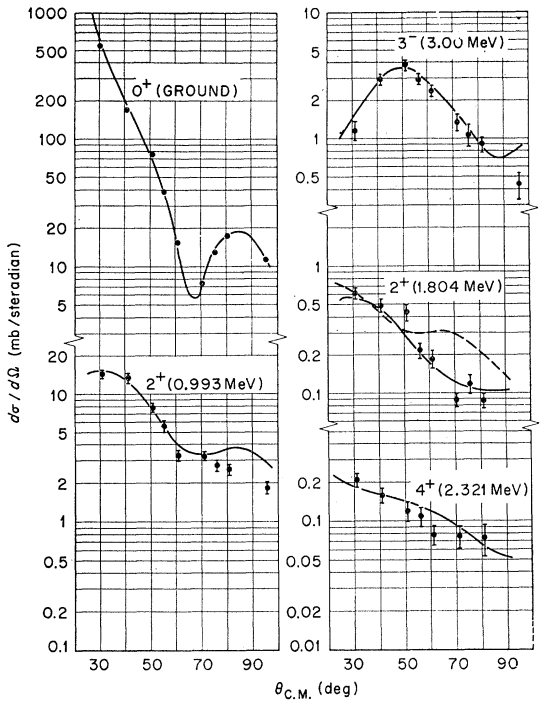

FIG. 20. Comparison of the theoretical and experimental cross sections of the scattering of 17.5-MeV protons by ^{64}Zn.

second excited 2^+ state was described as a small admixture of the one-phonon wave function to the dominant two-phonon wave function. On the other hand, a similar 0^+–2^+–2^+–4^+ coupling calculation in which the wave function of this 2^+ state is described purely in terms of the two-phonon wave function was performed, and the resulting cross section to this state is given as a dotted line. The difference between the solid and dotted curves, and the good agreement of the former with experiment is remarkable (although the latter type of calculation may give somewhat better agreement than is shown here, by searching for a better set of parameters.)

Whether the amount of the mixture of the one- and two-phonon wave functions in the former calculation was correct or not can be tested by calculating the ratio of $B(E2)$ values of the γ rays from the second 2^+ state to the ground state and to the first 2^+ state. The ratio is estimated to be 0.033 by using our wave functions, which is to be compared with the experimental value[51] of 0.007. Although there still exist differences of a factor of 5, they are of the same order of magnitude, and the agreement can be said to be very good. More systematic calculations along this line thus seem quite interesting.

In addition to improving and extending the sort of calculations reported in Sec. VII, many more other kinds of calculations can be made by using our formalism and the computer program. For example, some time ago we have discussed a possibility of performing the coupled-channel calculations in order to explain intermediate resonances observed in light nuclei.[52] A recent calculation made by Lemmer and Shakin[53] is very closely related to what we did, though there are some differences between their emphasis and ours.

As for slow neutrons, we have considered only 350-keV neutrons so far. We can certainly treat slower neutrons too and thus can compute the strength functions.[3,54] So far all the theoretical analyses of the strength functions were made assuming that the targets were of even-A, while the experiments were made by using both odd-A and even-A nuclei as targets. Experiments[55] seem to show that there is not any significant difference between the strength functions of even-A and of odd-A targets in deformed regions. The theory also predicts that this is true, at least if only the s-wave strength function is considered and the adiabatic assumption is assumed to be good. On the other hand, some question still exists[56] about the difference in the behavior of the strength functions for even-A and odd-A vibrational nuclei with $A\approx 50$. Since our code allows us to treat even- and odd-A nuclei differently, we can investigate whether such an odd–even effect would be expected theoretically, although perhaps very much care has to be exercised in the description of the target states in performing such calculations and deriving definite conclusions.

ACKNOWLEDGMENTS

The author is indebted to Dr. G. R. Satchler for his very kind interest, encouragement, and helpful discussions throughout the course of this work. He is also indebted to Dr. F. G. Perey for a number of stimulating discussions. Useful suggestions made by Dr. B. Buck and Dr. S. Okai in the initial stage of the coding of the computer program are highly appreciated. He thanks a number of experimentalists, Dr. J. K. Dickens, Dr. R. J. Silva, Dr. M. Sakai, Dr. G. C. Pramila, Dr. R. Middleton, Dr. R. Wagner, Dr. P. D. Miller, Dr. H. Marshak, and Dr. N. R. Roberson whom he had opportunities to work with, for their invaluable discussions and communications. He finally thanks Professor M. A. Melkanoff, Professor N. Austern, Professor J. S. Blair, Dr. P. H. Stelson, Dr. F. K. McGowan, Professor A. Bohr, and Professor B. R. Mottelson for valuable discussions.

[51] A. K. Sen Gupta and D. M. Van Patter, Nucl. Phys. **50**, 17 (1964).

[52] S. Okai and T. Tamura, Nucl. Phys. **31**, 185 (1962); T. Tamura, Phys. Letters **6**, 111 (1963); see also, D. E. Bilhorn and W. Tobacman, Phys. Rev. **122**, 1517 (1961).

[53] R. H. Lemmer, Phys. Letters **4**, 205 (1963); R. H. Lemmer and C. M. Shakin, Ann. Phys. (N. Y.) **27**, 13 (1964): See also, H. Feshbach, Rev. Mod. Phys. **36**, 1076 (1964).

[54] B. Buck and F. G. Perey, Phys. Rev. Letters **8**, 444 (1962); P. A. Moldauer, *ibid.* **9**, 17 (1962); A. P. Jain, Nucl. Phys. **50**, 157 (1964).

[55] See, e.g., R. E. Cote, R. F. Barnes, and H. Diamond, Phys. Rev. **134B**, 1281 (1964).

[56] W. M. Good and R. Wagner (private communication).